EVALUATION OF LONGITUDINAL CRACKING IN END REGIONS OF PRETENSIONED BOX BEAMS

by

Craig Morgan Chamberlain, B.S.C.E.

THESIS

Presented to the Faculty of the Graduate School of

The University of Texas at Austin

in Partial Fulfillment

of the Requirements

for the Degree of

MASTER OF SCIENCE IN ENGINEERING

The University of Texas at Austin

August 1997

EVALUATION OF LONGITUDINAL CRACKING IN END REGIONS OF PRETENSIONED BOX BEAMS

Approved by
Supervising Committee:

Michael E. Kreger

Ned H. Burns

To my parents

Acknowledgments

I would first like to thank TEXDOT for sponsoring this project. Several people have directly helped in providing any and all information that was needed. Special thanks goes to Keith Ramsey for tracking down old plans and documentation necessary for this project.

My supervising professor, Dr. Michael Kreger, has been an invaluable source of knowledge and information. He also deserves thanks for his patient and continued support of my work on this project. Dr. Ned Burns also deserves thanks for his contribution of insight and expertise into the nature of the problem investigated.

The Ferguson Structural Engineering Laboratory deserves a very big thanks. Their hands on expertise and commitment to lab safety help keep Ferguson running smoothly and efficiently. Blake Stasney, Wayne Fontenot, Mike Bell, and Raymond Madonna were extremely helpful with all testing activities.

Several graduate students helped in various ways along my journey in this project. I would like to thank Robbie Barnes for his help with testing logistics as well as cracking evaluation. My test team of Scott Jennings and Kevin Clinch also deserves credit for their help during each test without which I would have undoubtedly had many more problems.

Thanks goes especially to my family who have provided me with unconditional love and support in pursuit of my dreams. I would also like to thank my friends in Texas who have shown me that there is life outside of California.

Thanks ya'll.

Craig M. Chamberlain

Austin, Texas

August 1997

Abstract

EVALUATION OF LONGITUDINAL CRACKING IN END REGIONS OF PRETENSIONED BOX BEAMS

Craig Morgan Chamberlain, M.S.E.

The University of Texas at Austin, 1997

Supervisor: Michael E. Kreger

This study investigates the irregular, longitudinal cracking patterns occurring in bottom flanges of prestressed concrete box beams from the Hicks Road Overpass along U.S. Highway 287 in Tarrant County near Fort Worth, Texas. Testing of two, 65 foot box beams from the actual bridge was conducted to determine existing beam capacity and evaluate the cracking patterns.

Results from testing were analyzed and compared with current AASHTO standards. Longitudinal cracking was mapped and evaluated relative to the structural detailing. Past and current TxDOT standards were reviewed for box beam detailing and a recommendation was made for improved detailing of these box beams in the future.

Table of Contents

List of Tables

List of Figures

CHAPTER ONE: INTRODUCTION

1.1 BACKGROUND

Prestressed concrete design has been widely used in the United States since the 1950's and 1960's. As this design approach became more and more popular, research in the field grew. Early research focused on behavior of prestressed concrete members, while recent research has focused on implementing new materials in prestressed concrete design. While the behavior of prestressed concrete is generally considered to be well understood in the laboratory, observations from "real world" applications suggest there is more to be learned about prestressed concrete.

A prime example is the Hicks Road Overpass along U.S. Highway 287 in Tarrant County near Fort Worth, Texas. Constructed in 1976 with roadways to supplement the existing vehicular capacity, the overpass recently came under close scrutiny by Texas Department of Transportation (TxDOT) officials because of unusual cracking patterns in the bottom flange near the supports of many beams in the superstructure. The orientation and propagation of cracks in the bottom flange has perplexed officials. Cracks propagated along the bottom flange in a diagonal fashion, flaring from the central portion of the bottom flange near the support toward the webs of the box girder. Figure 1.1 shows an example of the observed cracking.

Figure 1.1: Cracking in bottom flange of box girder near support

Several theories were proposed by TxDOT engineers, but none conclusively explained the cause of these cracks. It was observed that some beams had moved laterally during recent years, disengaging the shear keys cast between the box girders. This implies that transverse post-tensioning strands through girder diaphragms were no longer effective, and beams were likely resisting applied loads individually instead of sharing loads with adjacent girders, as was assumed during design of the bridge superstructure.

TxDOT initially determined that regular monitoring of the bridge, rather than replacement, was the proper course of action, but by May, 1996 cracks had propagated to the extent (and at a rate) that structural integrity of the bridge was a concern. As a result, the bridge was demolished in June 1996.

TxDOT officials decided that a limited testing program incorporating girders from the existing bridge would provide information useful for estimating the capacity of existing bridges exhibiting similar, but perhaps earlier, signs of distress. Because large-scale testing can be performed at Ferguson Structural Engineering Laboratory at The University of Texas at Austin, two 65-foot beams from the overpass were transported to the laboratory for testing and subsequent analysis. An 85-foot girder from the bridge structure was also transported to Austin and was stored in a TxDOT maintenance yard.

1.2 OBJECTIVES

This study has two primary objectives. The first is to determine the shear capacity of the beams in their damaged state. As stated previously, this information will enable TxDOT engineers to estimate the capacity of bridge superstructures with similar damage. Because other bridges throughout the State of Texas have experienced similar cracking, this was a key component of the study. The second objective is to develop an understanding of the cracking mechanism. Determining the source of the observed cracking should facilitate

development of details to prevent this type of cracking or prevent propagation of the cracks in future box girder designs.

CHAPTER TWO: TEST PROGRAM

2.1 INTRODUCTION AND SCOPE OF TESTS

The experimental program consisted of testing two pretensioned concrete box girders from the Hicks Road Overpass on U.S. Highway 287 in Tarrant County near Fort Worth, Texas. The bridge was dismantled in June 1996 after TxDOT officials became concerned about excessive cracking observed in the ends of bottom flanges of the girders. Two 65-foot box beams were transported to Ferguson Structural Engineering Laboratory for testing.

The Hicks Road Overpass spanned a total length of 205 feet, and consisted of three spans of 65, 85, and 55 feet. Eleven box beams were used in each span, and were post-tensioned transversely at six interior diaphragms along the bridge. Traffic on the bridge was one-way and entered at the 65-foot-span end. A plan of the superstructure is shown in Figure 2.1.

Because observed cracking was concentrated at the ends of girders, bond of strand was likely affected, and as a result, so to was shear strength. The test program set out to evaluate shear capacity of the box beams in order to assess the capacity of other bridges exhibiting similar cracking. Two shear tests were conducted using different shear spans.

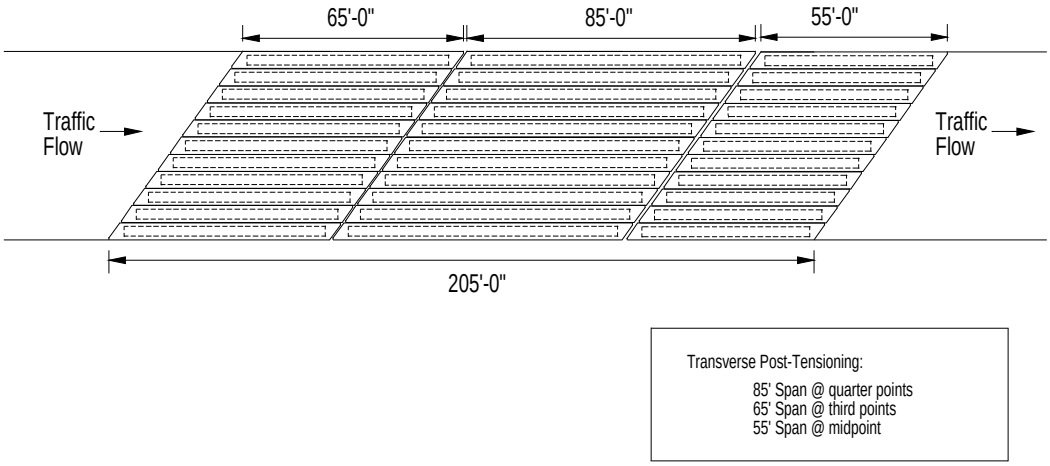

Figure 2.1: Superstructure Plan View

2.2 TEST SPECIMENS

2.2.1 Location of Existing Box Girders

TxDOT originally planned to deliver two of the outer 65-foot girders to The University of Texas (UT) for testing. These girders contained the most severe cracking, and likely were subjected to the highest truck loadings. However, during demolition these box beams were too severely damaged to be useful for testing. The least-damaged girders, which were delivered to UT for testing, were numbers three and five. Figure 2.2 illustrates the location of these beams.

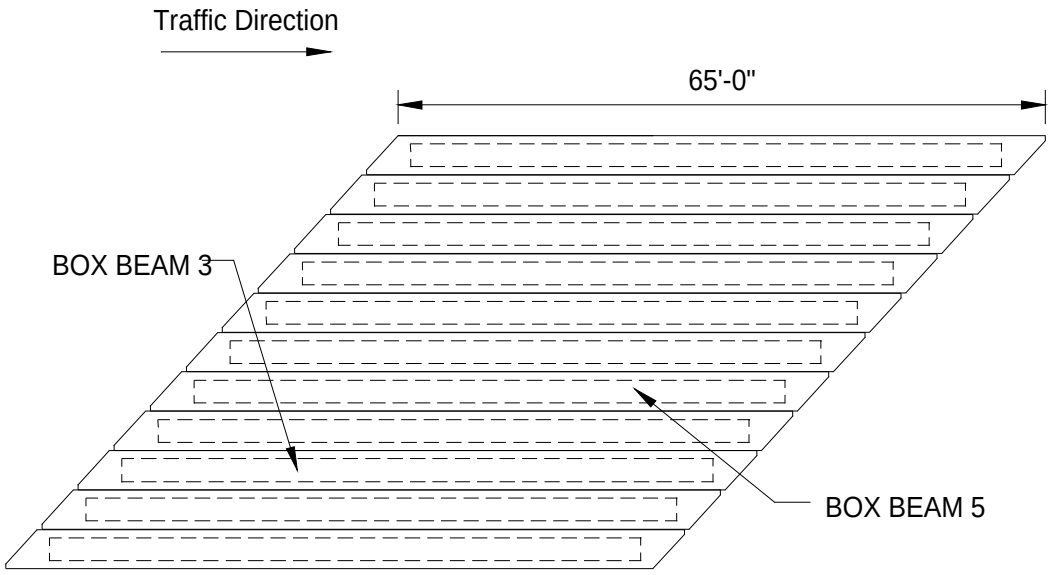

Figure 2.2: Location of Box Girders used in Test Program

2.2.2 State of Test Girders Before Testing

Unlike test specimens designed and constructed in the laboratory, the girders tested in this study were subjected to more than 20 years of service life before being tested. The beams had a thin layer of asphalt that was not completely removed from the top flange, and some of the cast-in-place shear key remained attached to one side of box beam five. However, this additional concrete was not in the region critical to shear strength of the girder.

All beams sustained various degrees of damage during disassembly of the bridge. Damage to the two girders tested in this study included cracking of the

top flanges, bent prestressing strand at beam ends, and concrete “punched” away from the outside of the bottom flange by the pneumatic demolition hammer.

Once the beams were transported to the Ferguson Structural Engineering Laboratory, it was determined the beams (and additional shear key material attached to the beams) combined with the lifting girder used to lift the beams at the appropriate locations were too heavy to be lifted by the 25-ton-capacity crane in the laboratory. As a result, the beams were shortened 12 feet by removing the most severely damaged end (damage imported during demolition) from each girder. A jackhammer and welding torch were used to sever the 12-foot section from each beam.

2.2.3 Beam Properties

Plans from 1974 that provided nominal dimensions as well as specified material strengths were obtained from TxDOT engineers. The box beams were designed using Class “H” concrete with a specified concrete strength at prestress transfer of 4000 psi and a concrete strength of 5000 psi at 28 days. Although 28-day cylinder breaks were not located, preliminary release strengths, listed in Table 2.1, were obtained from Mr. Joseph Roche of the Materials and Testing Division of TxDOT.

Table 2.1: Preliminary Release Strengths for Tested Box Beams

Box Beam Designation	Date Cast	Time after Casting	Cylinder 1	Cylinder 2	Average Comp. Strength
Box Beam 3 B1-HN402	9/8/75	18.5 hrs	6102 psi	6526 psi	6314 psi
Box Beam 5 B3-HN402	9/9/75	16.5 hrs	4775 psi	3944 psi	4360 psi

Longitudinal reinforcement included both prestressed and non-prestressed steel. The pretensioned reinforcement consisted of 24-½ in. dia. stress-relieved strands with a nominal ultimate tensile strength of 270 ksi. These strands were located in two layers of 22 strands in the bottom layer and two strands in the upper layer. Also typical to the design were six #9 Grade 60 bars for top-flange reinforcement.

The nominal girder cross-section was 28 inches in height by 47-¾ inches wide at the bottom and 43-¾ inches wide at the top. The box section had 5-inch thick webs and top and bottom flange thickness of 5-½ inches and 5 inches, respectively. A typical cross-section is shown in Figure 2.3.

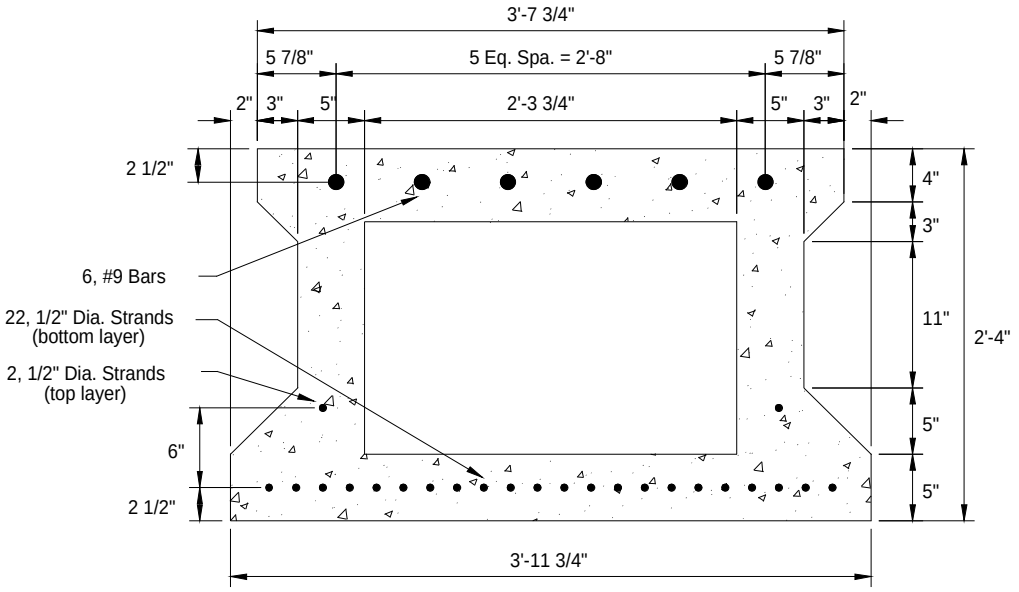

Figure 2.3: Typical Girder Cross Section

As indicated in Figure 2.1, the bridge was skewed 42 degrees, 10 minutes from a normal orientation. This required careful detailing of the solid, end-diaphragm regions. Figure 2.4 provides nominal plan dimensions of the solid end-diaphragm.

Transverse reinforcement was placed both parallel to the skewed end of each girder as well as perpendicular to the longitudinal axis. Three diagonal stirrups were placed at 1-½ in. from the end face of the beam (consisting of a combination of #4 and #5 bars), and 4-½ in. and 10-½ in. from the end face of the beam (consisting of only #5 bars). Stirrups in the end diaphragm and normal to the longitudinal axis of the beam were composed of two overlapping #4 bars that

formed a complete tie at 8-$^{5}/_{16}$, 16-$^{5}/_{16}$, 24-$^{5}/_{16}$, 36-$^{5}/_{16}$, and 48-$^{5}/_{16}$ in. from the far end location of each girder. Beyond this location, #4 stirrups/ties spaced at 1 foot on center were located around the hollow box section. All details for transverse reinforcement are shown in Appendix A.

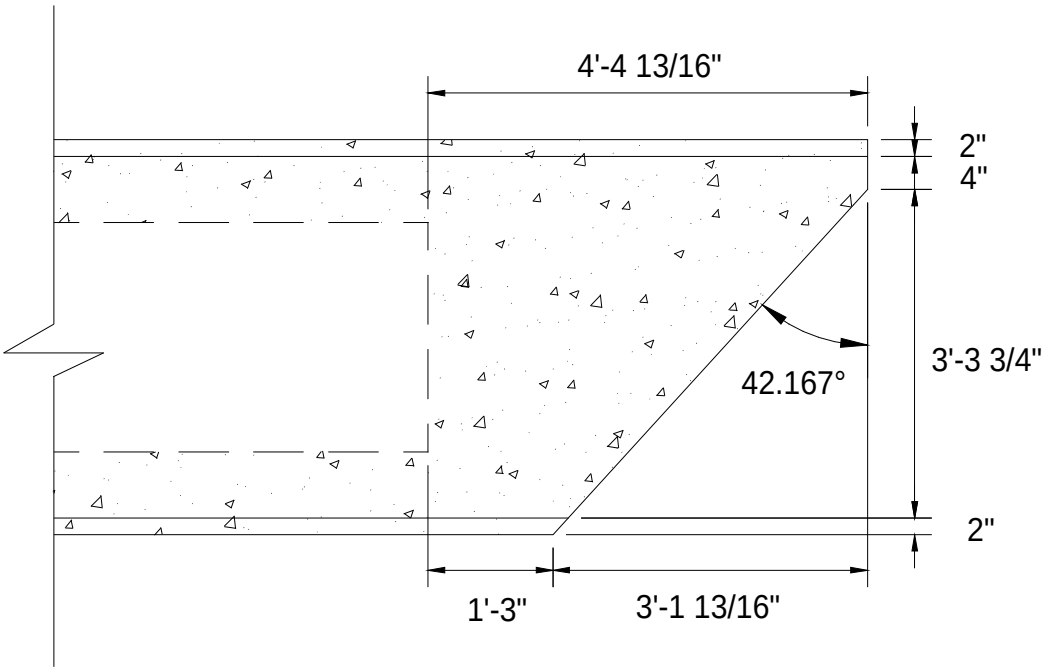

Figure 2.4: Nominal Plan Dimensions of End Diaphragm

Detailing of prestressing strands at the ends of girders included debonding of some strands. Of the 24 total prestressing strands, only eight strands, four on each outer side and both strands in the top layer were fully bonded the entire length of the beam. The remaining 14 strands, located in the bottom layer, were

debonded to two, four, and six feet from the girder end in the pattern shown in Figure 2.5. Original plans provided by TxDOT did not include the debonding pattern. Concrete cover was chipped away from one of the beams after testing in order to determine the exact locations of each debonding length used. Plastic sheathing was used to debond the strands, and this provided a readily identifiable indicator for locating the debonding locations.

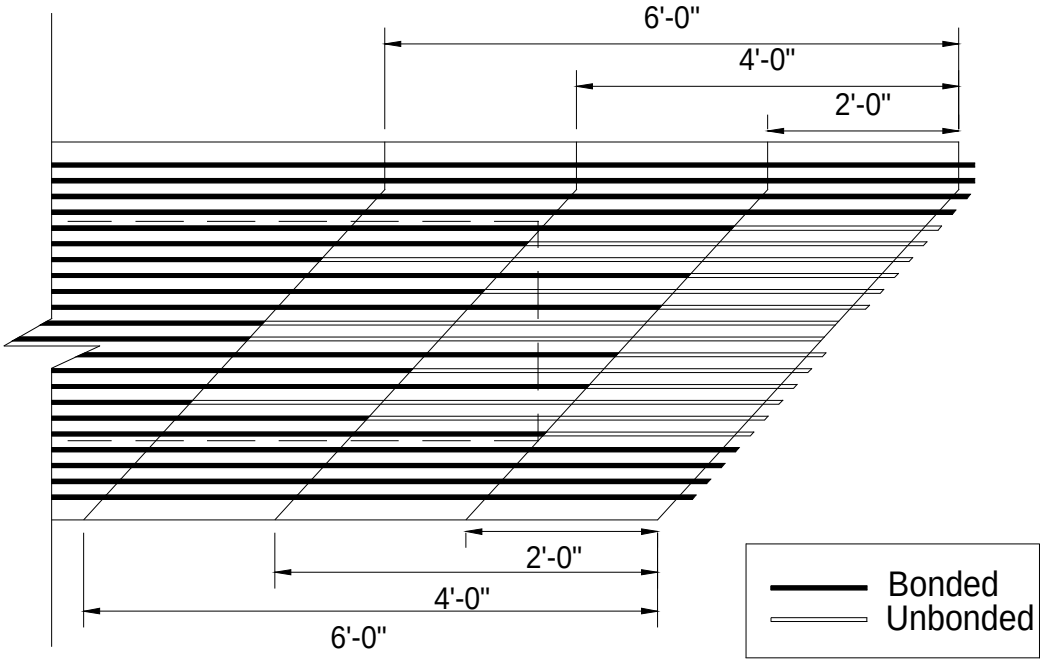

Figure 2.5: Strand Debonding Pattern

2.3 DESCRIPTION OF TEST SETUP

In order to assess the shear capacity of the girders, and to closely examine the cracking phenomenon observed in the end regions, the test setup focused on applying load near the useful end of each girder. Each girder was placed on 22 in. high concrete blocks and elastomeric bearing pads similar to those used in the actual highway overpass. By utilizing testing hardware available in Ferguson Laboratory, study costs were minimized. The only purchase necessary for assembling the test setup was the bearing pads.

2.3.1 Test Span and Loading Frame

Selection of testing hardware was related to the test span to be used, range of shear spans to be studied, and available space for the complete test setup. For the existing 53 foot section of beam available, several loading schemes were considered. The span had to be sufficiently short so that flexural failure did not preclude shear failure. Simultaneously, the span had to be sufficiently long so that shear failure would occur in the desired shear span. Based on an examination of shear and moment diagrams for various loading situations, and available laboratory space, a test span of 32 feet was chosen.

The minimum effective shear span, based on the shortest distance from the nearest loading point to the end of the voided section, was 42 in. A shorter shear

span would likely overestimate shear strength by transferring shear to the support via a more direct compression strut. Because two box beams were available for testing, a longer shear span of 84 in. was used for Test 2. The resulting minimum, effective shear span-to-depth a/h ratios for Test 1 and Test 2 (for "a" based on the distance from the end of the voided section to the nearest loading point) was 1.5 and 3.0, respectively.

The loading frame used in this study was developed for use in another study requiring similar loading conditions. The capacity of the frame was limited not by the frame itself, but rather by the structural slab to which it was attached. Each leg of the test frame was post-tensioned to the slab with 120 kips of force. The capacity of the frame was therefore limited to 480 kips, assuming equal distribution of loads to the four legs of the frame. A photograph of the loading frame and one of the girders is presented in Figure 2.6.

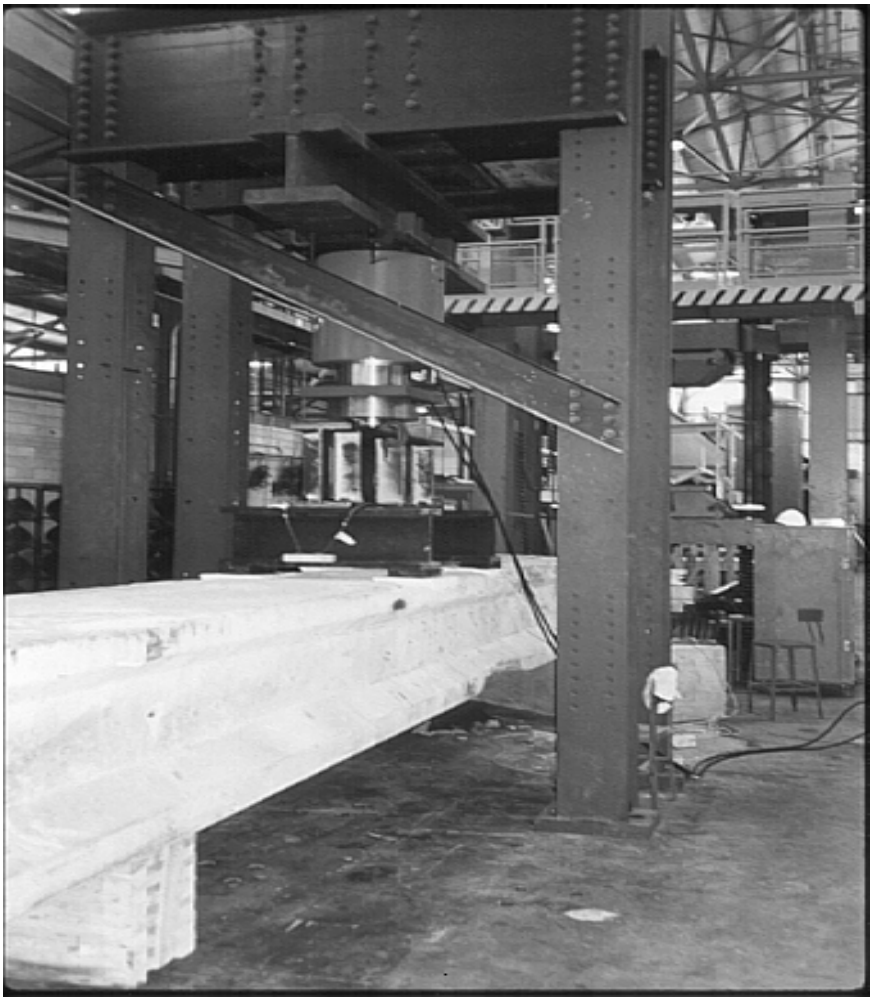

Figure 2.6 Loading Frame and Test Specimen

2.3.2 Truck Tandem-Axle Loading Simulation

In order to simulate the application of loads that were likely responsible for the cracking observed in the box beams, a spreader-beam assembly was fabricated to simulate a truck tandem-axle. In both the AASHTO 1996

Specification and the 1994 LRFD Specification, a four foot spacing is indicated for tandem-axle loading conditions [7,1]. In order to avoid punching through the top flange, the load was further distributed transversely into the webs. The resulting spreader-beam assembly applied loads to four locations as shown in Figure 2.7.

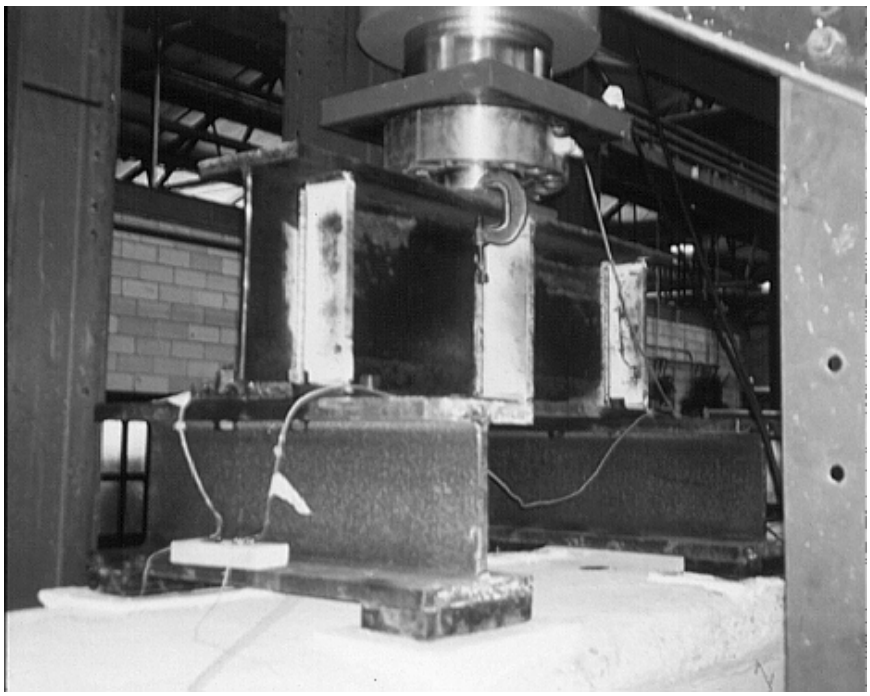

Figure 2.7: Spreader-Beam Assembly Simulating Truck Tandem-Axle

The spreader-beam assembly was designed for a maximum capacity of 480 kips. This required a W18x143 primary, longitudinal beam and two W12x162 secondary, transverse beams. The beams where bolted together at the

flanges, and web stiffeners were designed for the load transfer regions in the primary girder (these are visible in Figure 2.7).

Bearing pads were used for the transfer of load from the spreader-beam assembly to the box beam. These 6”x12” bearing pads were leveled using hydrostone to ensure proper load distribution. The hydrostone was also used to fill any cracks at these locations that were created during removal of the beams from the overpass.

The locations of the spreader-beam for each test are shown in Figure 2.8.

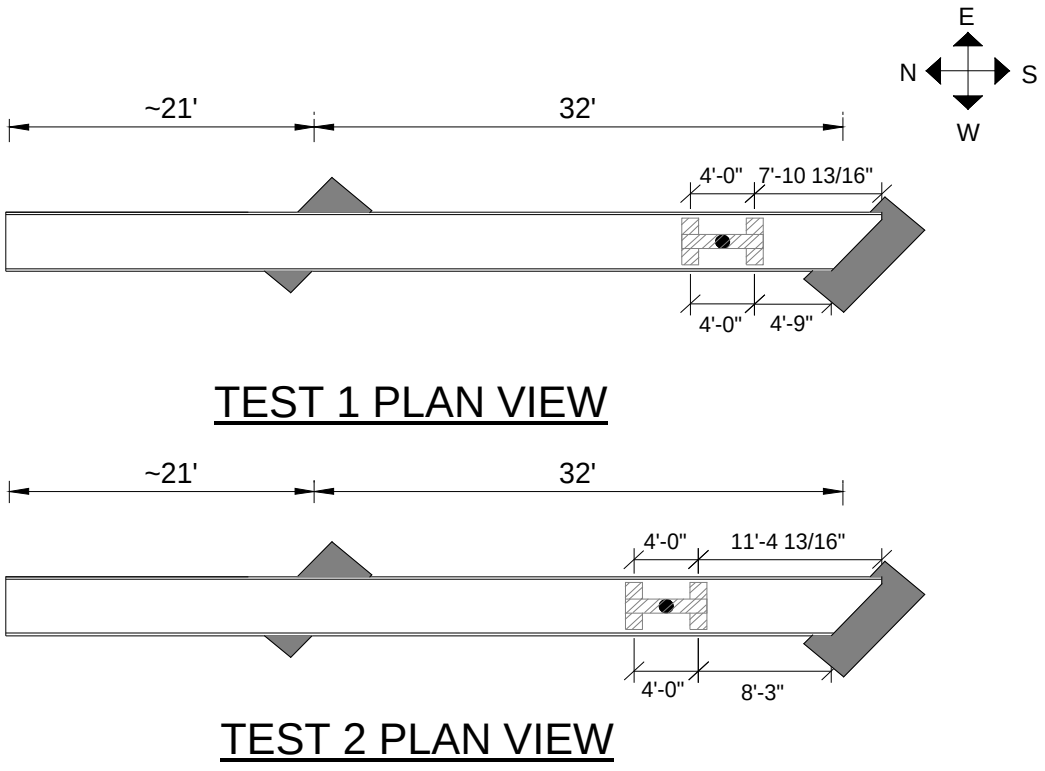

Figure 2.8: Location of Spreader-Beam Assembly for Test 1 and 2

2.4 INSTRUMENTATION AND DATA ACQUISITION SYSTEM

The instrumentation and data acquisition system assembled for each test were intended to monitor:

1) Applied Load
2) Deflection at midspan and near supports
3) Strand Slip near beam ends
4) Fiber Strains near the top of the beam at the location of maximum applied moment.

A total of 22 gages were used to monitor the actions described above during each test. Locations of all gages, except linear potentiometers to measure strand slip, are diagrammed in Figure 2.9. The locations of strand-slip gages are diagrammed later in this chapter.

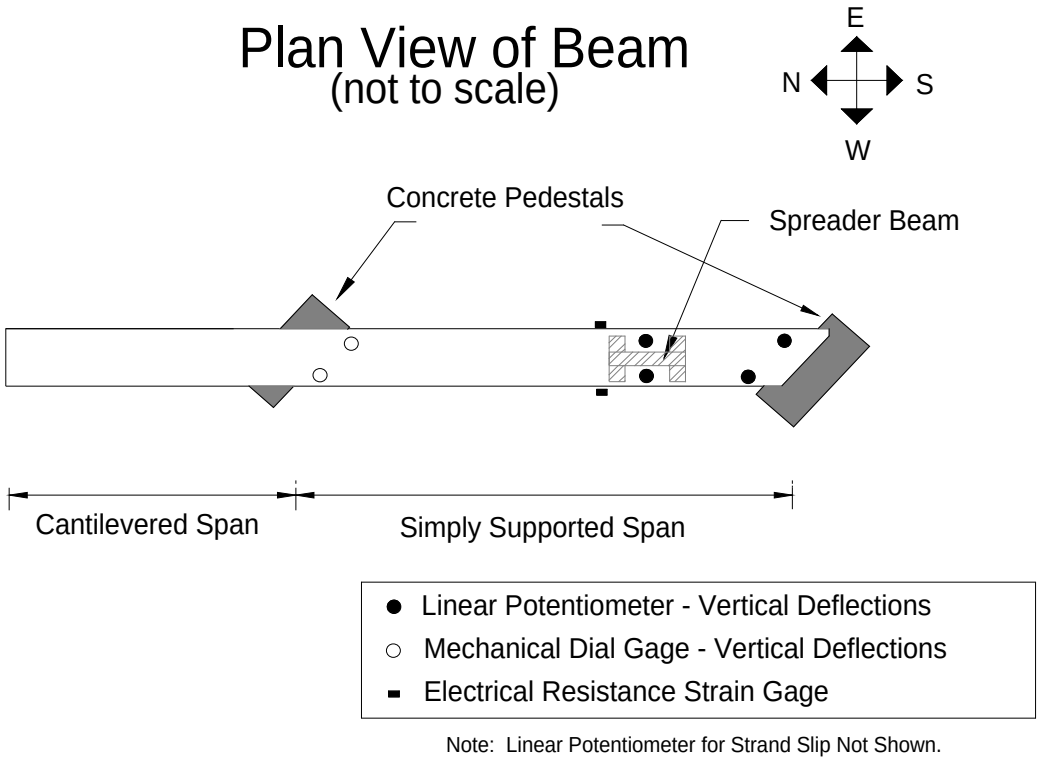

Figure 2.9: Deflection Instrument Locations

2.4.1 Load Cell and Pressure Transducer

Total load applied to the spreader beam during each test was monitored directly using a 1000-kip load cell. This load cell was connected to the bottom of the hydraulic actuator, and can be seen in Figure 2.6. The load cell was calibrated prior to testing.

A pressure transducer was used to monitor the actuator pressure during loading for safety precautions as well as to provide a backup measurement that

could be used to calculate the applied load had the load cell data been corrupted. The pressure transducer had a maximum capacity of 5000 psi and was attached directly to the hydraulic pump.

2.4.2 Deflection Gages

In order to examine deflections at different locations along the box beam, linear potentiometers, and mechanical dial gages were utilized. One linear potentiometer was placed beneath each web at the location midway between the two applied loads, and one was placed beneath each web as close to the nearest support as possible. One mechanical gage was placed beneath each web near the far support. Gages were placed in these locations to determine net deflections after the elastomeric bearing pads compressed. Two-inch linear potentiometers were used at the near support, while four-inch linear potentiometers were used beneath the applied load locations. Two-inch mechanical gages were used at the far support.

All deflection gages were mounted on stiff supports, and tips of each gage bore on smooth glass slides that were glued to the beam surface.

2.4.3 Strand-Slip Gages

Strand slip gages were used to monitor slip of the pretensioned strands that occurred during loading of each girder. Two-inch linear potentiometers were used to make these measurements.

On the end face of each girder prestressed strands extended a minimum of two inches beyond the face of the member allowing gages to be attached directly to the strands. The attachment of linear potentiometers to the strands was achieved using machined aluminum blocks that simultaneously clamped onto the strand and the linear potentiometer. A photograph of one gage is shown in Figure 2.10.

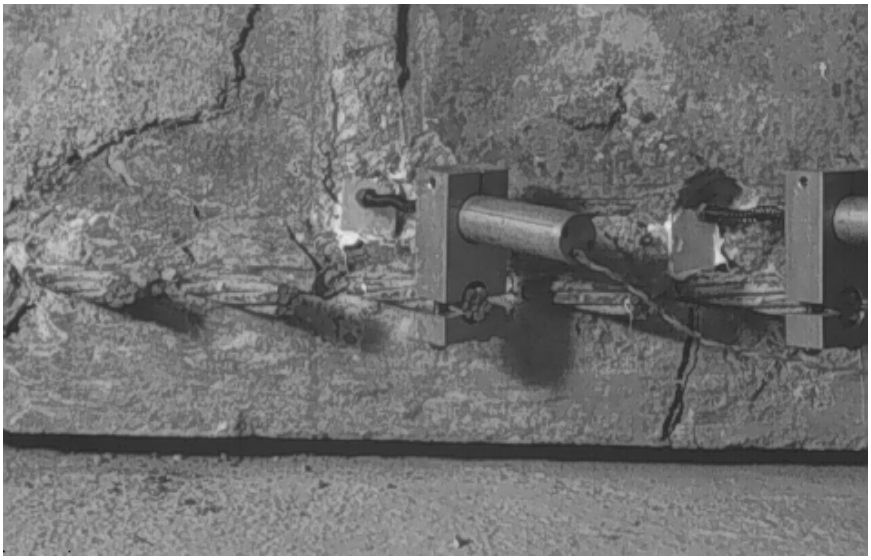

Figure 2.10 Strand-Slip Gage Device

Based on instrument availability, it was not possible to attach a linear potentiometer on each prestressed strand. Ten strands were monitored during testing. The majority of the ten that were monitored had the highest potential to experience slip. The locations of the ten linear potentiometers are shown in Figure 2.11.

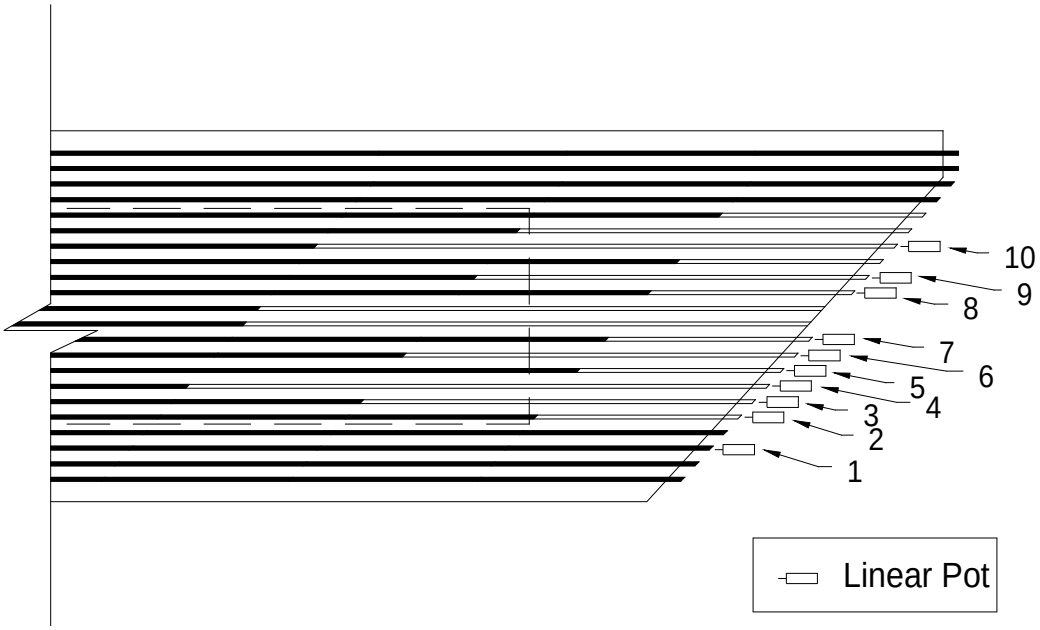

Figure 2.11: Location of Linear Potentiometers for Strand-Slip Measurements

Measurements of strand slip were difficult to obtain because the axes of the strands were not perpendicular to the end face of each girder; the vertical end face of the beam was skewed by more than 42 degrees. In order to accommodate

the skewed end, small (less than 1-in. diameter) holes were drilled in the vertical end-face of each member above the strands to be instrumented. These holes were then filled with silicon rubber, and a glass slide was placed into each hole, orthogonal to the longitudinal axis of the prestressed strand. Although silicon rubber is used primarily as a sealant, its thick, viscous characteristics worked well in fixing the position of each glass slide. After the silicon rubber hardened each slide was tested to make sure it did not deflect significantly under the pressure applied by the linear potentiometer. Glass slides can also be seen in Figure 2.10.

2.4.4 Strain Gages

External strain gages were used to approximately monitor maximum compressive strains near the location of maximum moment during testing. The gages were placed as near the top flange as possible. Because some damage to the top of each box beam had occurred, and it was desired to be consistent in the placement of the gages in each test, the gages were placed at $^{13}/_{16}$ in. above the bottom of the top flange.

Strain gages were required to be placed on flat surfaces, and therefore the location along the length of the beam was varied between tests because of existing damage in the girders. Test 1, using Box Beam 3, had a strain gage attached to each side of the box beam beneath the center of the Northernmost applied load. While this would have been the optimal choice for Test 2 as well,

damage to Box Beam 5 prevented this. Strain gages were placed on each side of the beam three feet past the center of the Northernmost applied load.

2.4.5 Data Acquisition System

Collecting and storing data for analysis was accomplished using a COMPAQ personal computer and a Hewlett Packard high-speed scanner. The scanner converts the analog measurements from instruments mounted on the specimen to digital output which is relayed to the computer. The personal computer controls the scanner, converts the electronic data to engineering units, and stores the data on the hard drive. The software program used for data acquisition is called HPDAS, and was developed by staff at the Ferguson Structural Engineering Laboratory.

Instrumentation on the specimen was connected to the scanner through "Front End Boxes" that contain the electronic components necessary to form either quarter or full-bridge circuits. In this study all gages were attached to full bridge Front-End Boxes except for the strain gages which were attached to quarter bridge Front-End Boxes. An excitation voltage was connected to each Front-End Box.

An X-Y plotter was used during testing to monitor progress of the tests. The plotter was connected directly to the output of the load cell for the vertical readings (Y axis) and to the east vertical displacement potentiometer for

horizontal readings (X axis). Calibrations were then made to monitor a load vs. deflection plot during testing. Figure 2.12 is a photograph of the data acquisition system used in the study.

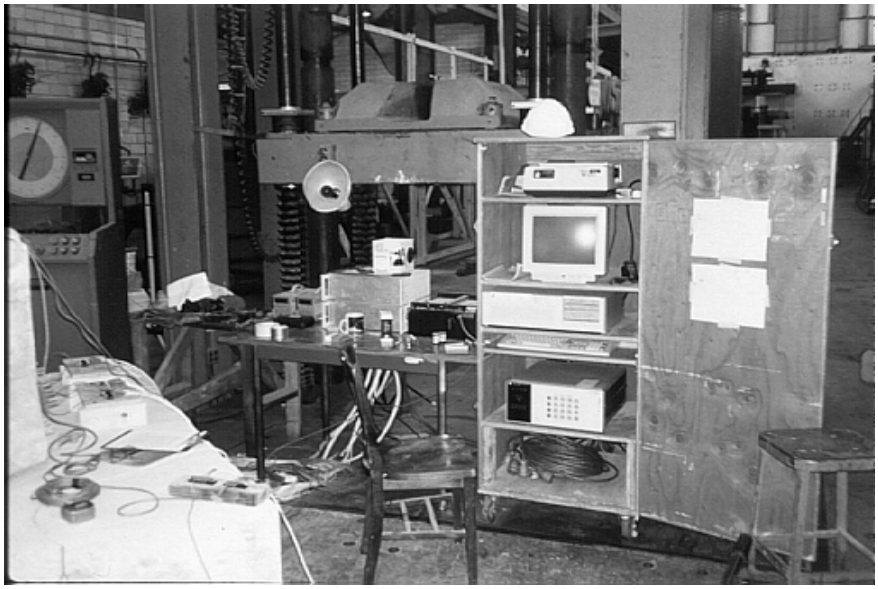

Figure 2.12: Data Acquisition System

2.5 TEST PROCEDURE

Because both girders had incurred damaged previously in the field, identifying marks to distinguish new cracks during testing versus existing cracks were needed. Existing visible cracks were marked with a red felt-tip marker before any load was applied to each girder. Cracks that developed or became visible during testing were marked with a black felt-tip marker. Load levels were noted adjacent to cracks when cracks were marked.

After all instrumentation was in place, and before actual testing was initiated, several preliminary steps were taken. The first step was to zero all channels in the data acquisition and then to perform a "scan check" of all channels to confirm that the computer was correctly reading output from the instruments. Three small increments of load were than applied to qualitatively verify the output from all gages. Actual testing began after zeroing the gages again and performing a "scan check".

Each test proceeded with initial load increments of 10 kips. The load was monitored via the plotter and was applied using an electrically powered hydraulic pump. At each load increment all channels were scanned and a hard copy of the readings was obtained with a printer. The data was stored in the memory of the personal computer. The two mechanical dial gages at the North support were read and recorded manually after each load step. Photographs were taken of significant crack propagation during testing. Cracks were marked at intermittent load steps. Widths of the most significant cracks were also measured at some points using a hand-held crack-width comparator when cracks were marked. At higher load levels, subsequent load increments were not applied until audible cracking ceased. As the load-displacement behavior of each girder became more nonlinear, the magnitude of successive load increments was reduced. Channels were scanned at each increment. Each test was discontinued when significant damage had occurred and when the beams were unable to resist the previously-attained maximum load. Final photographs of the damaged specimens were taken, and a final scan of all channels was performed prior to completely unloading each beam. Load was slowly removed from each specimen, then a

final scan of all channels was performed. Testing of each girder required approximately five to six hours to perform.

Following each test, data stored on the personal computer were transferred into spreadsheet format. Crack mapping of the bottom flange near the loaded end was also performed once load was removed from each beam.

CHAPTER THREE: TEST RESULTS

3.1 INTRODUCTION

Testing of the box beams was performed in April 1997 and consisted of two tests conducted within a five-day period. Each test was conducted as described previously in Chapter Two. Data reduction was accomplished using Microsoft Excel Software. Cracking patterns and only data deemed pertinent to evaluation of the box-beam capacities are presented here. Strain gages provided no significant, useful data, and as a result, no strain data are presented.

3.2 TEST 1 - BOX BEAM 3

3.2.1 Observations

Testing was performed on April 11, 1997, and began with successive load increments of 10 kips. At approximately the 169-kip load level, significant cracking in the West web occurred. Load on the specimen fluctuated around this level as deflections increased throughout the remainder of the test. The maximum load level attained was 175 kips. When it was apparent that the box beam had been pushed beyond its capacity, the test was terminated.

Because of the short effective shear span in this test, much of the observed new cracking was the result of web-shear cracking. All web-shear cracks were observed outside the solid end diaphragm in the hollow, box section of the beam. As would be expected, the web-shear cracks originally occurred on the short side (West side) and did not develop on the long side (East side) until much later in the test. Cracking patterns in the webs and bottom flange are presented later.

Almost no flexural cracking was observed. Only one flexural crack under the loading ram on the long side (East side) of the girder was noted near the conclusion of the test. A flexural crack would be expected to initiate on this side because of the longer shear span. This crack propagated less than halfway across the width of the bottom flange.

Test 1 data for Box Beam 3 is tabulated in Appendix B.

3.2.2 Load and Deflection Data

As described above, load was initially applied to the specimen in 10-kip increments. During the test the deflection response to these load increments appeared to be linear until 169 kips, at which point significant spalling of concrete in the West web began to occur. Because of the damage that was developing in the girders, load was not maintained between load steps. Drop in load was typically on the order of 5 to 10 kips. If possible, the specimen was reloaded 5 to 10 kips during the next load increment, or to a point where significant cracking or strand slip had occurred. Instrument readings were collected each time loading

was stopped. Testing ended when it was obvious the beam was not resisting additional load but was accumulating significant deflections.

Beam deflection was monitored at six points along the bottom flange of the box beam as described previously in Chapter Two. Deflections were recorded beneath the load point and near the two bearing pads for both the East and West sides of the beam. The effect of bearing pad deflections at the load point were subtracted out of the load-point deflections to generate "actual" deflections corresponding with the load increments.

Load versus deflection plots were generated for the data, and help to explain an observation during the test that was alluded to earlier in Section 3.2.1. It was observed that the web on the West side of the beam carried much of the load until web spalling initiated in the web. Some of this load was then picked up by the East side web. Figure 3.1 shows the "actual" West and East load-point deflections. The plot demonstrates that the East deflections were slightly larger than the West deflections up to 169 kips. The higher stiffness of the West side response is consistent with the shorter shear-span. Larger bearing pad deformations were also observed on the West side, and are indicative of the larger percentage of load resisted initially by the West web. After the 169-kip load level was reached, the "actual" East deflection curve rapidly increases while the West load-point curve appears to no longer deflect under successive load increments. The West load point was actually experiencing nearly equal deflection measurements at the linear potentiometers at the load point and at the bearing pads near the loading frame. Damage experienced by the East web for load

increments beyond the 169-kip level was indicative of the increasing percentage of load being resisted by the East web.

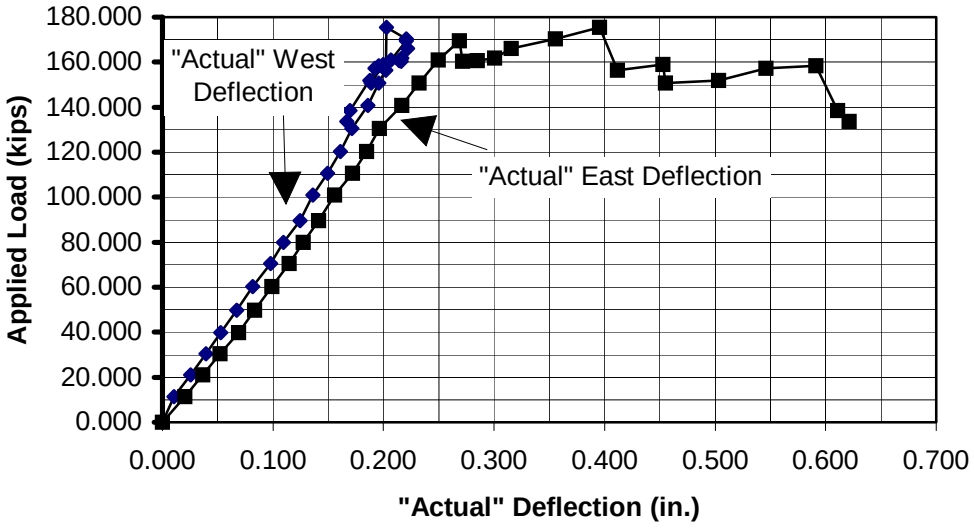

Figure 3.1: Load vs. "Actual" West and East Load-Point Deflections for Test 1

An attempt was made to demonstrate the overall load vs. deflection response for this girder by averaging the two "actual" West and East deflection records as shown in Figure 3.2. Because of the skewed beam end and unequal East and West shear spans, care must be taken in the interpretation of this data. The purpose of this plot was to demonstrate a general load-versus-deflection response for the beam. The maximum deflection, as plotted here, was 0.39 inches at the final load step of 133.5 kips.

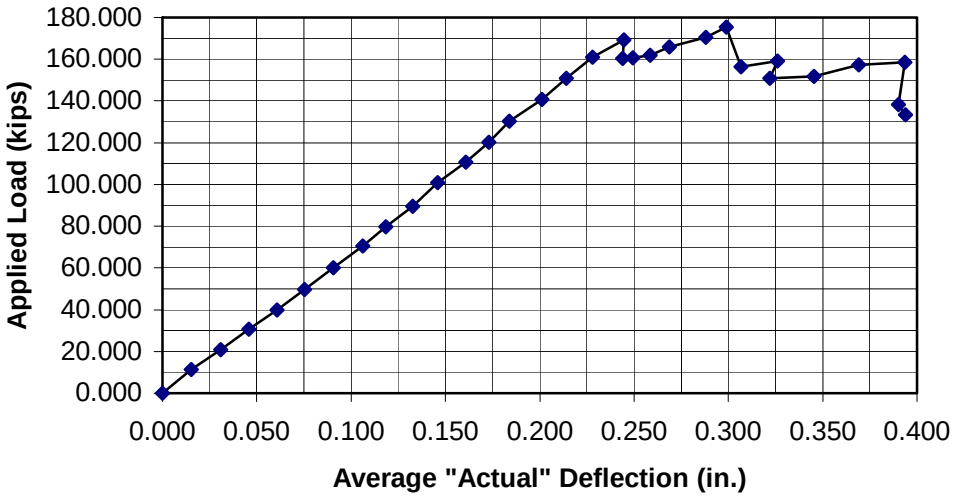

Figure 3.2: Load vs. Averaged Load-Point Deflections for Test 1

3.2.3 Strand Slip Data

Monitoring the relative displacement of the ends of prestressing strands during the test provided important data. Little to no slip was detected in any of the monitored strands (see Figure 2.11) until the 169 kip load level was reached when all monitored strands except Strand #1 registered slips of several hundredths of an inch. For the remainder of the test, strands slipped during nearly every load increment. Figure 3.3 displays the maximum measured slip for each monitored strand. Strand #2 had the largest slip of nearly ¼ inch.

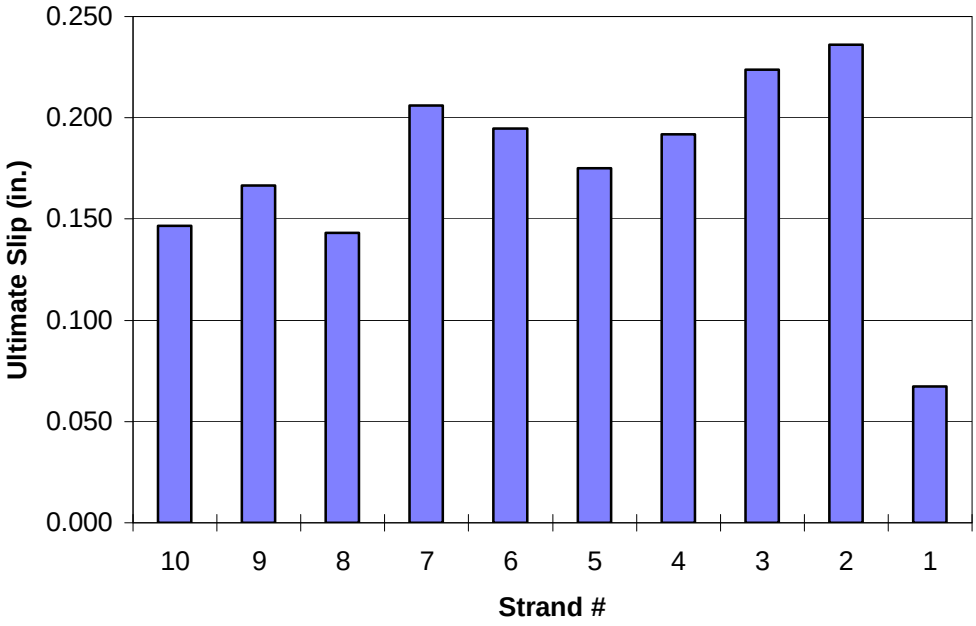

Figure 3.3: Maximum Measured Slip of Monitored Strands During Test 1

Slip of the strands during the test never exceeded three hundredths of an inch in any one load increment. Accumulation of slip over the remaining load increments past the 169 kip load level is the maximum slip illustrated in Figure 3.3. A general increase in strand slip was observed from Strand #10 to Strand #2. It is likely Strand #1 did not follow this pattern because it was fully bonded.

After the test was completed, the linear pot on Strand #5 was found to be bent and not functioning properly. Although data collected for this strand was similar to the other strands, it may not be reliable. Close examination of the data for Strand #5 revealed little except for a negative initial reading as testing began.

This suggests that the strand may have experienced more slip than reported in Figure 3.3. However, this additional slip was only on the order of a few thousandths of an inch, at most.

3.2.4 Crack Propagation

Two cracking patterns were monitored during the test. The first and most important were those that occurred on the underside of the beam (where cracks were visible in the field). The second pattern which was directly related to the applied load on the beam, was the web-shear cracks that formed on each side of the beam.

Prior to testing, existing cracks were marked on the box beam with a red felt-tip marker. Figures 3.4 and 3.5 show this cracking in the web and bottom flange on both sides of the beam. These figures also display some of the existing damage to the girder prior to testing.

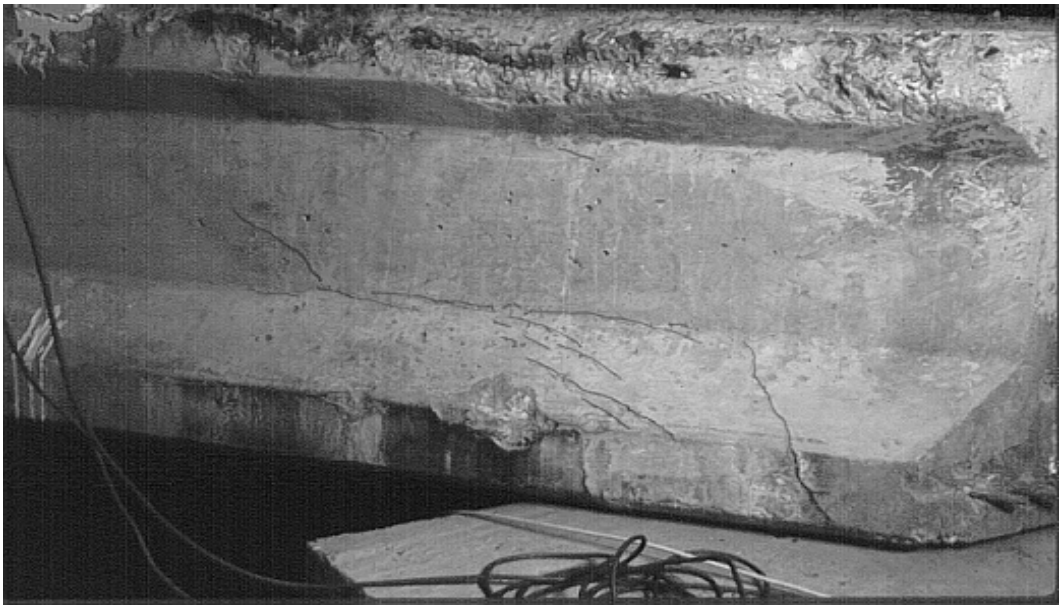

Figure 3.4: Pretest Cracking of West Face of Box Beam 3 - Test 1

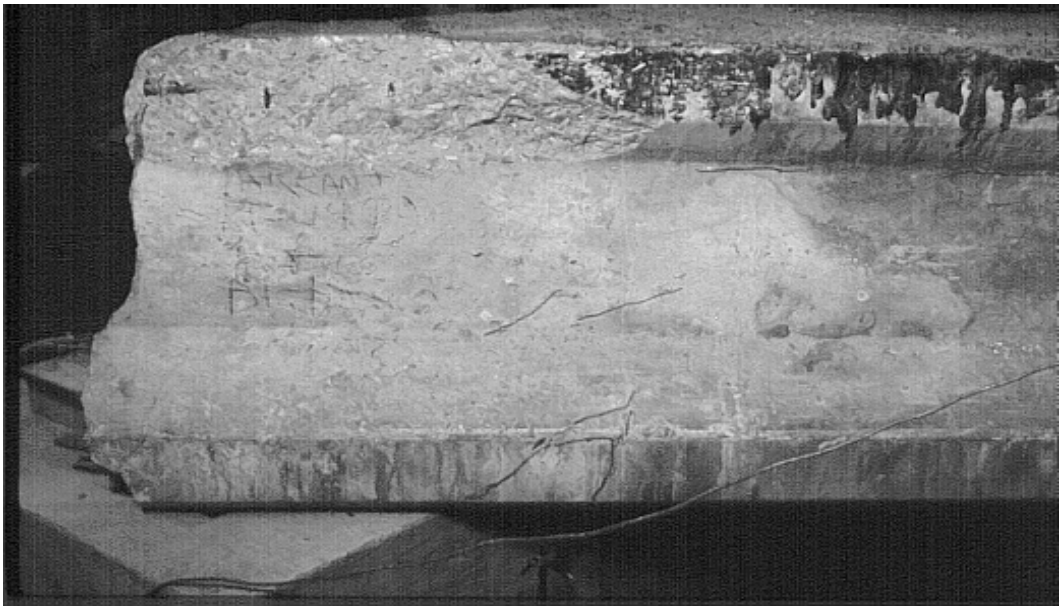

Figure 3.5: Pretest Cracking of East Face of Box Beam 3 - Test 1

Upon loading of the girder, cracks began forming in the West web first. It should be noted that web shear cracks opened at loads substantially lower (80 to 90 kip level) than computed cracking loads, suggesting that the cracks already existed and were opened by the applied loads. After substantial web-shear cracking in this web, the East web began to experience web-shear cracks as well. All web-shear cracks originated in the hollow, box section before propagating into the solid end diaphragm. Figures 3.6 and 3.7 illustrate the cracking and spalling in each web at failure. Note the well-defined "band" of cracks from the spreader-beam to the support on the West side of the beam. The maximum crack width in this web at failure was approximately ¼ inch.

Figure 3.6: Cracking and Spalling at Failure on West Face of Box Beam 3

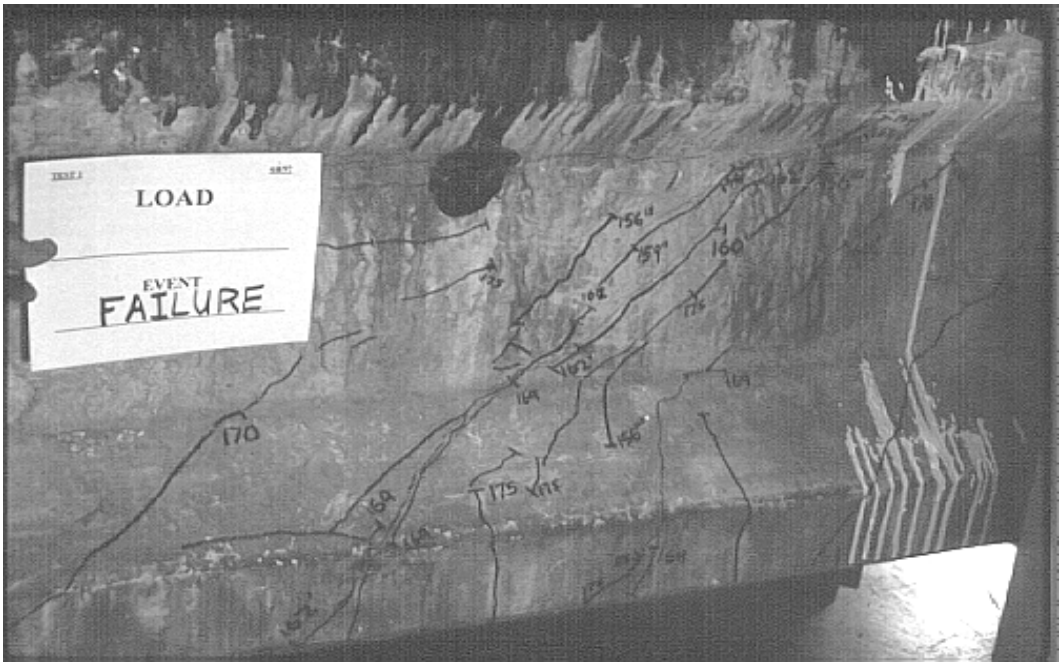

Figure 3.7: Cracking and Spalling at Failure on East Face of Box Beam 3

Cracking of the underside of the box beam is mapped in Figure 3.8. Some of these cracks did not originate during the testing; they existed before testing. Only one crack at the 169 kip load level appeared to propagate from an existing crack and flare out toward the edge of the beam as previously observed in many of the box beams. The remaining cracks were caused by slip of the pretensioned strands, and propagation of the shear-flexure cracks on the East side of the girder. Cracks in this region were also observed to widen as testing proceeded, with the existing crack on the East underside reaching 0.1 inch.

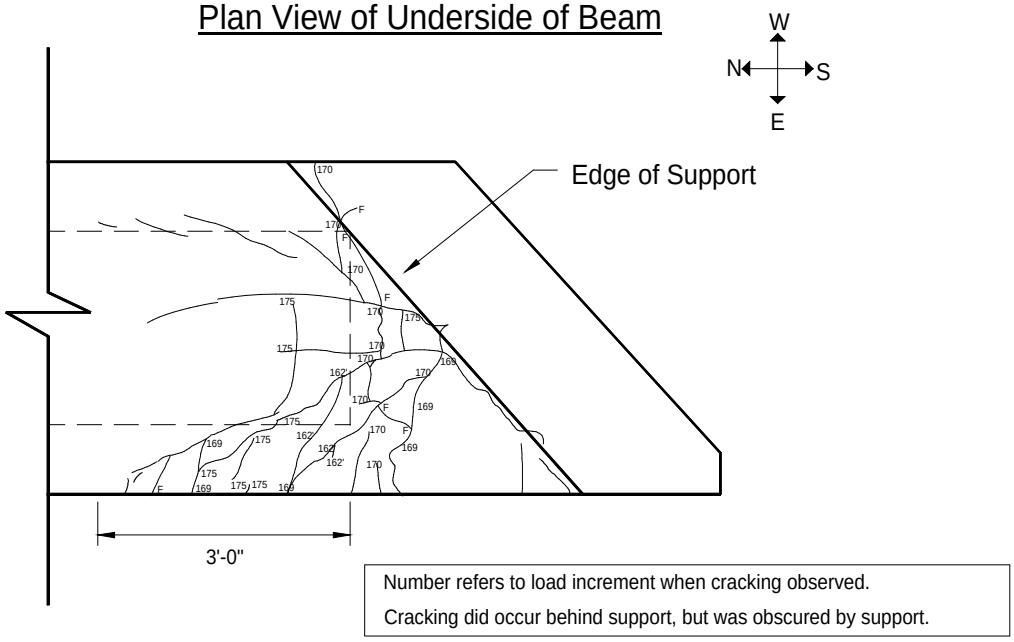

Figure 3.8: Crack Map of Beam Bottom Flange - Test 1

3.3 TEST 2 - BOX BEAM 5

3.3.1 Observations

The second test was performed on April 15, 1997. The nearest loading point on the West side of the spreader-beam assembly was now moved to three times the depth of the section beyond the beginning of the box section. As for the first test, gages were ensured to be working properly before the actual test began. Ten kip load increments were again initially used in this test. Little damage was evident on the box beam up to 120 kips when small web-shear cracks propagated

from existing cracks. The 10 kip load increments were used through the 210 kip load level, at which time the first significant web spalling occurred and the applied load fell off slightly. At this point the specimen was loaded in 5-kip increments. The maximum load achieved was 231 kips. At the very next attempted load increment, loud cracking and popping noises emanated from the damaged end of the beam. Loading was stopped and after several minutes under the applied load, the West web and portions of the top and bottom flange suddenly failed in compression.

The longer shear span utilized in this test developed a different cracking pattern. As in Test 1, web-shear cracks formed, but unlike Test 1, flexure-shear cracks also formed during Test 2. Cracks again occurred outside the solid end diaphragm, and cracks appeared on the West side of the beam before the East side.

Unlike Test 1, a large number of flexural cracks were distributed evenly throughout the bottom flange in the loading region. The first crack originated under the ram and propagated across the entire bottom flange. Cracks in the webs and bottom flange of the girder at failure are presented in a later section.

Test 2 data for Box Beam 5 is tabulated in Appendix C.

3.3.2 Load and Deflection Data

Regular load increments of 10 kips were used through two-thirds of the test while five kip or smaller load increments were used during the last third of

the test when strand slip required small reload increments to reach the maximum load of 231 kips. All instruments were scanned immediately after failure occurred, and after load was removed from the girder.

Deflection instruments were placed in the same locations as in Test 1. Although unnoticed during the test, the linear potentiometer monitoring the East bearing pad at the South end appeared to have slipped during the test at the 216 kip load level. This likely occurred as a result of someone bumping the stand while marking cracks on the bottom flange. This possible error was on the order of a tenth of an inch and was not removed from data.

The West side of the girder appeared again to attract more load than the East side, although not as significantly as during Test 1. In fact the ram appeared to be loading the West side of the spreader-beam more than the East side, but the load appeared to distribute more evenly after some load had been applied to the box beam. The initial unequal loading was likely caused by poor leveling of the spreader-beam assembly on the girder, and by differences in the shear span for the East and West side.

Bearing pad deformations on the East side of the beam for the South and North ends supports the observation that load was initially directed toward the West web. Table 3.1 shows the initial deflection of these bearing pads. It is logical to assume that because the loading points are closer to the South end than the North end of the beam, the bearing pad deflections would be greater at the South end than the North. This was not the case, as demonstrated in Table 3.1 where bearing pad deformations were approximately the same. The North pad deformation actually became larger than the South at the 120 kip load level. This

suggests that much of the load from the ram was directed into the West web. Bearing pad deformations for the West pad at the South end agree with these observations when compared against East pad deformations at the South end.

Table 3.1: Test 2 Bearing Pad Deformations for East side of Beam

Load Step	Load (kips)	South End Bearing Pad Δ (inches)	North End Bearing Pad Δ (inches)
0	0.00	0.000	0.000
1	11.39	0.035	0.025
2	20.98	0.062	0.045
3	30.92	0.085	0.065
4	40.41	0.109	0.085
5	51.15	0.131	0.106
6	61.25	0.152	0.127
7	70.84	0.169	0.147
8	81.13	0.184	0.167
9	90.62	0.194	0.183
10	100.71	0.207	0.201
11	110.70	0.218	0.218
12	120.84	0.229	0.237
13	131.38	0.239	0.257
14	141.27	0.251	0.277

As for Test 1, load vs. deflection plots were produced. The "actual" East and West deflections were more similar for this test than for Test 1. The East side began to deflect significantly more than the West near the 200 kip load level, and reached a maximum differential of more than 0.4 inches at the final load step. Figure 3.9 illustrates the load-deflection plots for the East and West sides of the girder.

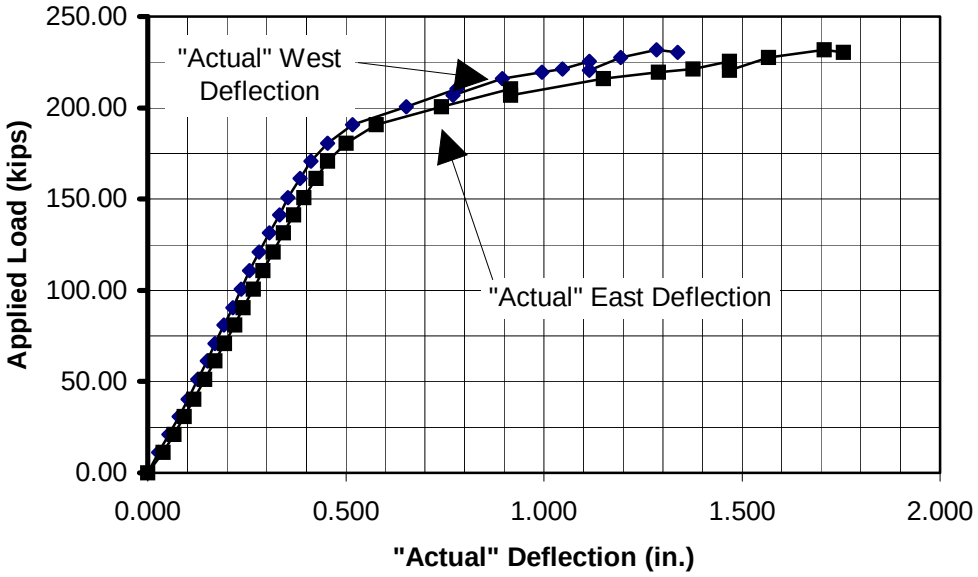

Figure 3.9: Load vs. "Actual" West and East Load-Point Deflections for Test 2

The maximum deflection from the average of the East and West responses was 1.56 inches at the final load of 230.5 kips.

3.3.3 Strand Slip Data

Prestressing strands were monitored at the same locations as in Test 1, and as indicated in Figure 2.11. Little noticeable slip occurred until the 200 kip load level. At the next load step (210 kips) all instrumented strands except Strand #1 demonstrated an increase in slip of approximately 0.01 inches. This slip

increased as the test progressed and reached 0.015 inches for Strand #4 at the final load step of 230.5 kips. As described earlier, testing was discontinued here when the specimen failed. Large slips were recorded for most of the strands when failure occurred. The linear potentiometer on Strand #1 fell off at failure because of the severe slip experienced by the strand. Figure 3.10 shows a photograph of the twisting of the strands and gages during slip at failure of Strands #1-7. The maximum slip recorded by the linear potentiometer was 0.44 inches for Strand #2, but the slip on Strand #1 (where the gage fell off the strand) likely exceeded this value. Figure 3.11 displays the maximum slip for each monitored strand.

Figure 3.10: Rotation of Strand Slip Gages at Failure of Box Beam 5 - Test 2

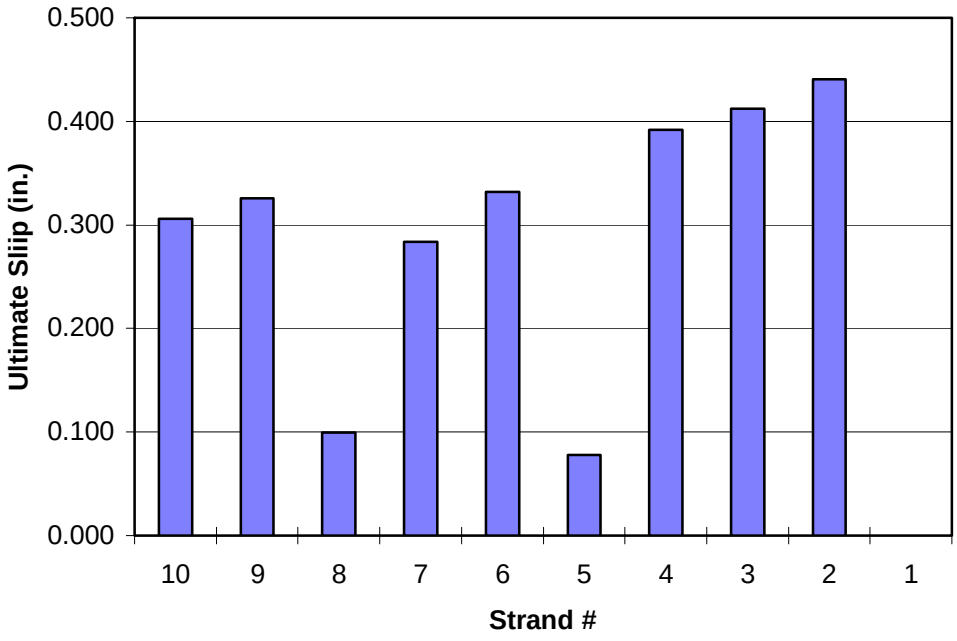

Figure 3.11: Maximum Slip of Monitored Strands in Test 2

The slip of any one strand did not exceed 0.03 inches during any load increment before the last attempted load step. The accumulation of slip during the entire test for each instrumented strand is the maximum slip recorded in Figure 3.11. Note that no slip is shown for Strand #1, however the strand actually slipped enough to remove the gage from the strand.

A trend of increasing slip appears to have occurred from Strand #10 to Strand #1. This did not occur for gages #8 and #5 where significantly lower slip was recorded. At the end of the test it was noted that the gage on Strand #5 appeared to have slipped.

3.3.4 Crack Propagation

Test 2 developed web-shear cracks, flexure-shear cracks, flexural cracking, and splitting cracks on the underside of the beam. All cracks noted prior to any loading were again marked with a red felt-tip pen, and pretest cracks for the West face are illustrated in Figure 3.12. Pretest cracks were not visible on the East face of the girder.

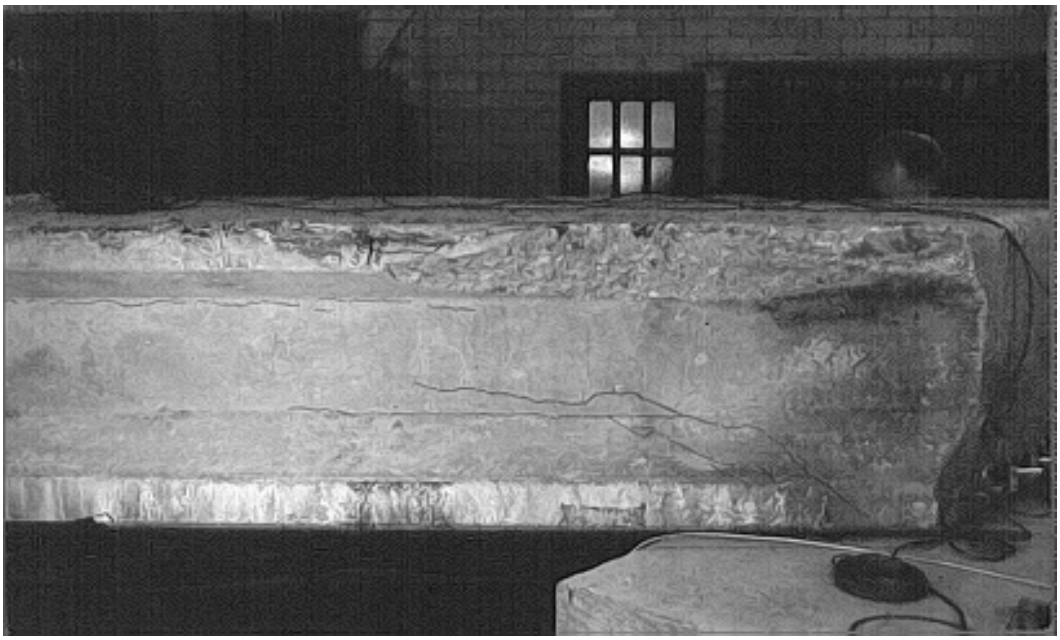

Figure 3.12: Pretest Cracking of West Face of Box Beam 5 - Test 2

Web-shear cracks were first visible on the specimen on the West side of the beam, and at 120 kips an existing crack began to widen and propagate. The original width of this crack was approximately three thousandths of an inch, but faulting became apparent at 180 kips. Just before failure the crack width had reached nearly six hundredths of an inch. From this first crack, a well-distributed "mesh" of web-shear cracks formed during the test. At failure (232 kips) crushing formed in the region of the web-shear cracking. Figure 3.13 shows a photograph of the West side of the beam at failure where concrete crushing in the web and flanges was prevalent.

Figure 3.13: Concrete Crushing on the West Face at Failure of Box Beam 5

Flexure-shear cracks were also visible during this test. Many of these cracks propagated from flexural cracks that developed in the bottom flange. This cracking was visible on both sides of the beam at 200 and 210 kips. The cracks propagated from the region of web-shear cracking to the closest point of load application. Figure 3.14 shows a photograph of the East side of the beam at failure where flexure-shear cracking was prevalent.

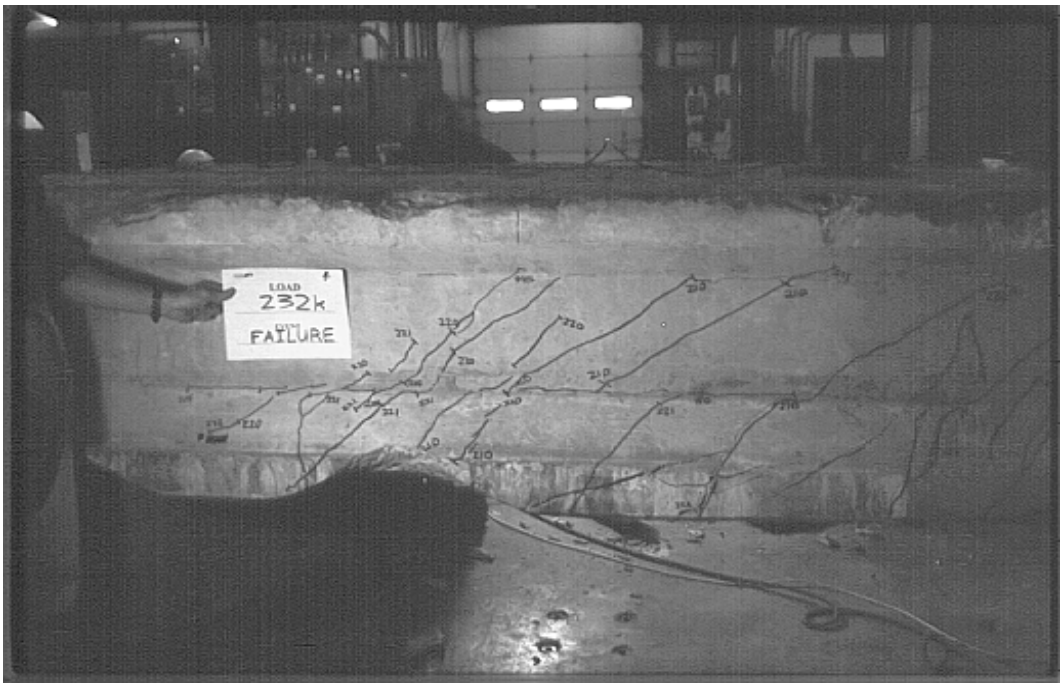

Figure 3.14: Cracking Pattern at Failure on East Face of Box Beam 5

Flexural cracking began at 180 kips with a crack beneath the loading ram that propagated the entire width of the bottom flange. The flexural cracks were also well-distributed on both sides of the loading frame. These cracks propagated into the inclined-shear cracks as mentioned above, as well as into the diagonal cracks on the underside of the beam.

Figure 3.15 shows a crack map of the underside of the beam. Unlike Test 1, these cracks were observed to propagate during loading. Multiple diagonal, flaring cracks, as well as extensions of existing cracks were evident. The first, new cracks appeared at the 210 kip load level and were observed to extend at each load step beyond this. Faulting and spalling of concrete occurred in this region. The three other types of cracking mentioned in this section joined with these cracks on the underside of the girder.

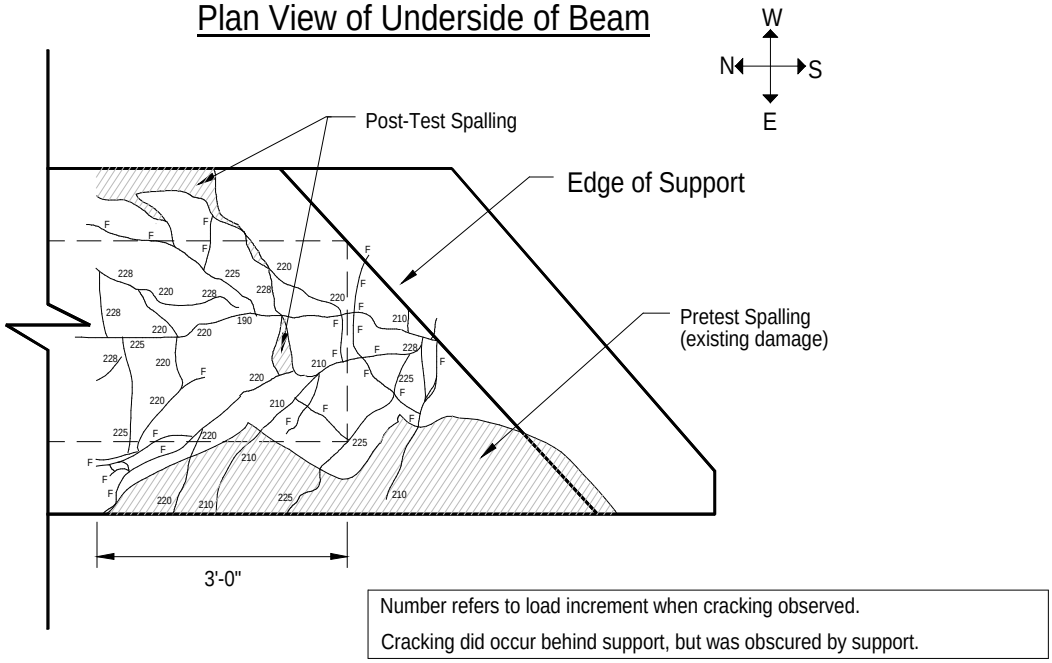

Figure 3.15: Crack Map of Beam Bottom Flange - Test 2

3.4 SUMMARY OF RESULTS

The results of the two tests are summarized in Table 3.2. Each test experienced web-shear cracking, and the second test also developed flexure-shear cracks and pure flexural cracking. Both box beams were tested to failure. Substantial strand slip occurred in both tests by the time structural failure occurred. Although not observed in Test 1, Test 2 developed cracks on the underside of the beam similar to those observed in other girders in the field and similar to those observed in Beam 3 before it was loaded.

Table 3.2 Summary of Box Beam Tests

Test	Test 1 - Box Beam 3	Test 2 - Box Beam 5
1st Concrete Spalling *(kips)*	169	210
1st Major Stand Slip *(kips)*	169	210
Maximum Applied Load *(kips)*	175	231
Maximum Strand Slip *(inches)*	0.236	0.440
Strand #	2	2

3.5 SUMMARY OF NONDESTRUCTIVE TESTING

On August 13, 1996, M. Sansalone, R. Poston, and K. Kesner performed Impact-Echo testing [3] on the end regions of an 85-foot box girder that was also removed from the Hicks Road Overpass but stored in a TxDOT maintenance yard in South Austin. The bottom flange of the girder contained some of the most extensive cracking observed in any of the girders (see Figure 3.16).

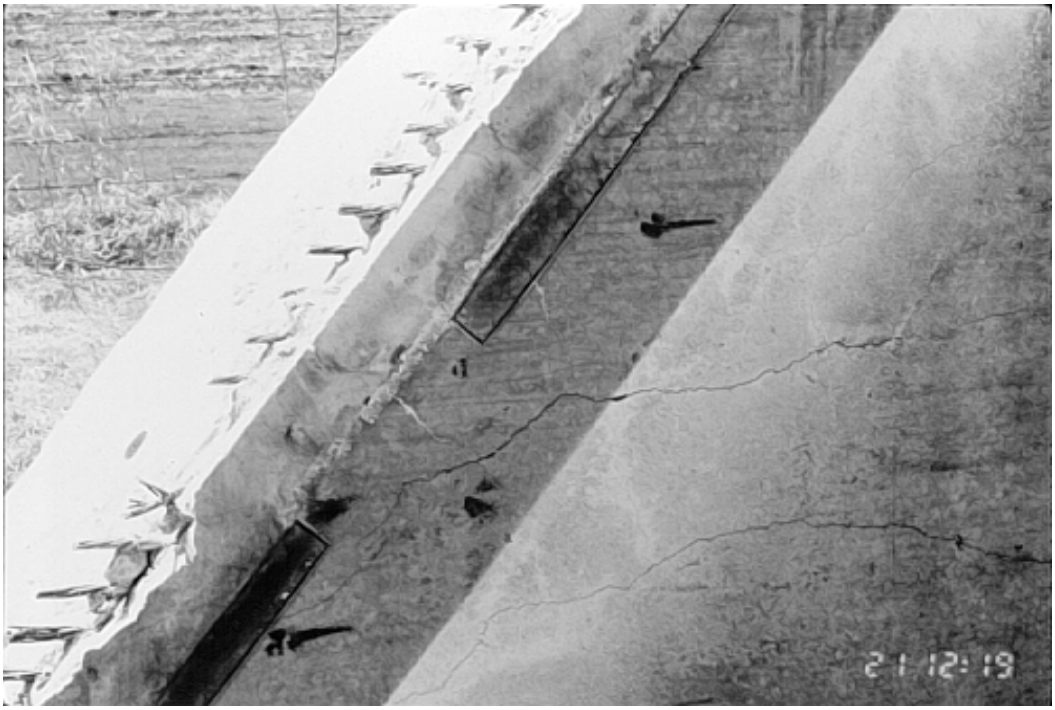

Figure 3.16: Cracking of 85-foot Box Beam used for Impact-Echo Testing

The nondestructive (impact-echo) testing was performed to determine whether the observed cracks were normal to the bottom-flange surface or inclined with respect to the surface (such as a crack surface formed as the result of splitting in the plane of the strands). Tests revealed that the cracks propagated normal to the surface, and cracks beneath the box-girder void penetrated the full depth of the bottom flange.

CHAPTER FOUR: EVALUATION OF TEST RESULTS

4.1 INTRODUCTION

This chapter analyzes the results of each test by comparing the measured capacities of the box beams with code-required capacities. It begins by explaining how the skewed end of the box beams was treated analytically. The chapter then examines the required shear strength of the beams according to AASHTO Specification [7] and compares this strength with the estimated capacity of the box beams, as designed. The capacity of the box beams is estimated using the 1996 edition of the ASSHTO Specification for web-shear (V_{cw}), flexure-shear (V_{ci}), and pure flexural capacities. Flexural behavior is also evaluated using a moment-curvature analysis developed by Lin and Burns [4]. Once the required capacity and estimated capacities have been compared, each test will be examined for its performance relative to the analyses described above. Comments regarding the probable cause of failure will be made here as well.

4.2 APPROXIMATION USED IN ANALYSIS OF SKEWED BOX BEAMS

This section explains the method used to consider the effect of the 42°10' skew at the end of the box beams. The exact approach for analyzing a beam with a skewed end would be to analyze cross sections parallel to the end face. Within

the solid end diaphragm of the beam this might be an acceptable approach, but once the hollow section of the beam is encountered on one side of the current section being considered, the cross section with irregularly placed stirrups and ties becomes quite complex.

In order to simplify analysis of the girders, an attempt was made to treat the beams as if no skew existed at the ends. Analysis of the box beams provided a reasonable approximation of the moment and shear values along the length of the simply supported beam. This approximation specifically affected the analysis for applied loads during testing, and analysis of the dead load in AASHTO calculations discussed in the next section.

Figure 4.1 shows the approximate box beam with non-skew ends, and details the location of the hollow box section. Values for the distributed load in each region are also presented. The length of the solid end diaphragm was found by measuring the length of the actual end diaphragm along the centerline of the box beam. By subtracting the two end diaphragm lengths from the total length of the beam, the length of the hollow box section was determined. Dead loads for the box section and end diaphragms were calculated based on a density of 150 pcf. The distributed dead loading values shown in Figure 4.1 correspond to the dead load of the beam only and do not include shear key concrete or any asphalt topping on the box beam.

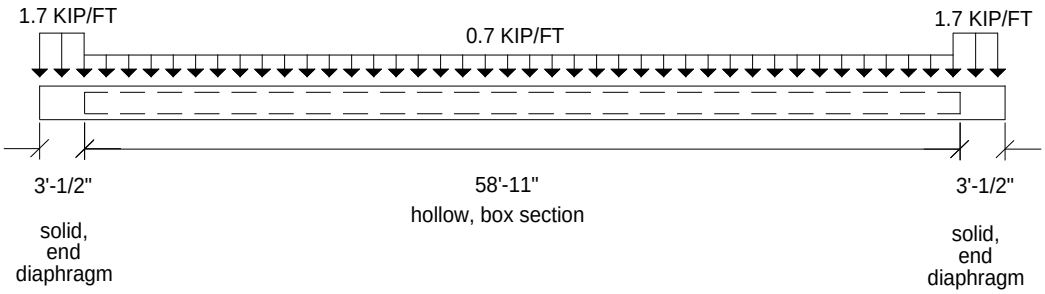

Figure 4.1: Approximation of Box Beam for Analysis

4.3 ASSESSMENT OF BOX BEAM CAPACITY

Capacity requirements for the girders were computed based on current AASHTO Specifications, then were compared to estimated section capacities computed using AASHTO Specifications equations. Load and Resistance Factor Design equations were emphasized in the computation of required capacities. Two key assumptions were made and are used consistently throughout these analyses. Although original plans specified a 28-day concrete compressive strength of 5000 psi, actual strength of the concrete at present is very likely higher than this. A value of 6500 psi was chosen and was conservatively extrapolated from concrete strength data obtained at release of the prestressing strand. The other assumption involved the estimation of prestress losses. The effective prestress was taken as 60% of the nominal ultimate strength of the prestressing strand (162 ksi).

4.3.1 AASHTO Specification Required Capacity

Most bridges constructed today are designed according to AASHTO Specification requirements. For many years the "Standard Specification for Highway Bridges" was the primary document for bridge design standards, but recently (1994) a new, LRFD Bridge Design Specification was published. This section will examine both the requirements of the sixteenth edition of the Standard Specification for Highway Bridges (1996) and requirements of the first edition of the LRFD Design Specifications (1994) [7,1]. The purpose of this comparison was to determine the minimum current strength requirements for the box beams.

In addition to considering both of these specifications, the analysis for required capacity was approached in two different ways. As discussed in Chapter 1, several key observations were made prior to dismantling the bridge. Cracks in the wearing surface over the joints between beams were evident, as shown in Figure 4.2. This suggests that box beams had moved laterally, implying the transverse post-tensioning through interior diaphragms had lost effectiveness. Standard Specification Article 3.23.4.1 states that shear keys and ties must provide adequate interaction to ensure proper load distribution. The observed separation of girders, which approached one-quarter inch in some cases, indicates the beams were likely acting independently. To consider a worst-case scenario, analysis included a condition where one wheel line bore directly on a single beam. This represented the extreme overload case where half the weight of a

truck bore directly on a single beam. The other condition simply involved a check of a standard loading distribution along the bridge assuming the requirements of Article 3.23.4.1 were met.

Figure 4.2: Longitudinal Cracks in Wearing Surface of Bridge Deck

Three specific analyses were conducted to determine the capacity requirements, and Table 4.1 summarizes the results. The first two cases assumed

total lack of box beam interaction, as described above, and used the two specifications mentioned previously. The third case assumed of adequate box beam interaction and utilized the sixteenth edition of the Standard Specification for Highway Bridges.

Basic load combinations were used in each case. Specifically, the load combination from the Standard Specification for Highway Bridges was Group I = 1.3[1.0D + 1.67(L + I)]. The variables D, L, and I, refer to dead load, live load, and impact load, respectively. Dead load was similar to the loading illustrated in Figure 4.1, except that an increase of 0.25 kip/ft was added along the beam to represent shear key concrete. The live load used was the standard HS20-44 truck loading. Impact loading used is specified in Article 3.8 of the specification and is expressed as a fraction of the live load. The impact load in this case was 26.3% of the live load.

The LRFD Bridge Design Specifications are similar to the Standard Specifications. A basic load combination was again chosen and is classified in this document as load combination STRENGTH I = 1.25DC + 1.75(LL + IM). The variables DC, LL, and IM, refer to the dead load of structural components, vehicular live load, and vehicular dynamic load allowance, respectively. The dead load used in this equation was the same as that described above. Live load was calculated based on either a "design lane load" and "design tandem" or a "design lane load" and "design truck". Impact loading was specified in Article 3.6.2 as 33% of the live load, but was not applied to the "design lane load".

Table 4.1: Summary of AASHTO Required Capacities

	LRFD AASHTO 1994		STANDARD AASHTO 1996		STANDARD AASHTO 1996	
	Lack of Box Beam Interaction		Lack of Box Beam Interaction		Adequate Box Beam Interaction	
	Service Load	Factored Load	Service Load	Factored Load	Service Load	Factored Load
V_{DL}	33.10	41.38	33.10	43.03	33.10	43.03
V_{LL}	41.25	72.19	30.85	66.98	20.33	44.14
V_{IM}	10.18	17.82	8.11	17.61	5.35	11.61
V_{TOT}	84.53	131.39	72.06	127.62	58.78	98.78
M_{DL}	490.5	613.1	490.5	637.7	490.5	637.7
M_{LL}	616.2	1078.4	448.0	972.6	295.0	640.4
M_{IM}	147.8	258.7	117.8	255.7	77.6	168.5
M_{TOT}	1254.5	1950.2	1056.3	1866.0	863.1	1446.6

Units of V are in kips.
Units of M are in ft-kips.

The factored-load-based required strengths summarized in Table 4.1 are the minimum requirements for shear and flexural capacity of the box beams. Notice the required strength for the case where box beam interaction was assumed. These values are significantly lower (22 to 26% lower) than when no interaction was assumed. The two specifications used to analyze the case of complete lack of box beam interaction produced similar results, with the LRFD Specification producing slightly higher required shear and moment capacities.

4.3.2: Estimation of Shear Capacity According to AASHTO Specification

Shear capacity near the end regions of the box beams was estimated using AASHTO provisions. Section 9.20 from the 1996 AASHTO Standard Specification for Highway Bridges was used to evaluate both the web-shear and flexure-shear capacities. Based on a preliminary analysis, web-shear capacity was found to control in the region in question, therefore only data pertaining to web-shear calculations are presented here.

Calculating a reasonable estimate of the shear capacity near the end of the box beam proved to be a difficult task for several reasons. The skewed end again entered into consideration. Cross sections parallel to the end face should have bean evaluated, but were not for reasons described previously. An additional difficulty was placement of transverse reinforcement, both parallel to the end face of the beam as well as perpendicular to the longitudinal axis of the beam, as shown in Appendix A. Another factor adding to the difficulty of assessing shear strength was the arrangement of debonded prestressed strands. Web-shear capacity is partly a function of the amount of prestress, and in the end region where strands were not only debonded, but were also staggered, determining the level of effective prestress at any section was difficult.

Shear capacity was estimated using cross sections perpendicular to the longitudinal axis of the beam. Figure 4.3 demonstrates a sample calculation. Shear capacities calculated in this way were associated with the centerline location on the girder so they could conveniently be compared with required

strengths computed by AASHTO provisions. For example, the computed capacity of 154 kips associated with the beginning of the box section was attributed to the centerline location of 36.5 inches. This is the same location as the beginning of the box section in Figure 4.1. Other nominal shear capacities for sections near the beam end are summarized in Table 4.2. Note that shear capacity increases with distance from the end. This is due to the increasing effective prestress force that accumulates as debonded strands become effective. Values are not reported within the first three feet of the beam (where the end diaphragm is located) because shear strength was substantially greater in this region.

Effective prestress in each strand was determined by multiplying the ratio of the actual bonded length beyond the section of interest to the required transfer length ($25d_b$), by the effective prestress at full transfer. Obviously, strands that were bonded $25d_b$ or more were considered fully effective.

Table 4.2: Centerline Shear Capacity Estimate based on AASHTO 1996.

Centerline Distance from Beam End (inches)	V_N (kips)
36.5	154
42.5	160
48.5	165
54.5	167
60.5	170
66.5	173
72.5	176
78.5	179
84.5	181

Shear Capacity Estimate:

- The estimated shear capacity at the interface of the solid end diaphragm and box section is calculated. The concrete contribution to shear capacity is estimated by AASHTO equation 9-29:

$$V_{cw} = \left[\frac{3.5\sqrt{f_c'}}{1000} + 0.3f_{pc} \right] b'd$$

Section Properties:

b'=	10 inches (summation of two webs)	f_C'=	6500 psi (assumed)
d=	25 inches	f_s'=	270 ksi (TEXDOT plans)
A=	680 in^2 (hollow, box section)	f_{se}=	162 ksi (0.6*f_s')

Step 1: Summation of F_{se} (following AASHTO Section 9.20.2.4):
Of the total 24 prestressing strands, 5 fully bonded strands are completely developed, 5 fully-bonded strands are partially developed, and all 6, two-foot debonded strands are partially developed. All 8, four and six-foot debonded strands are still debonded (ineffective) at this cross section.

A summation of the prestress forces at this section gives: F_{se}= 301 kips

Step 2: Calculation of f_{PC}:

$$f_{pc} = \frac{F_{se}}{A} = \frac{300.72}{679.375} = \underline{\underline{0.433 \text{ ksi}}}$$

Step 3: Calculate V_{CW}:

$$V_{cw} = \left[\frac{3.5\sqrt{6500}}{1000} + (0.3)(0.433) \right](10)(25) = \underline{\underline{104 \text{ kips}}}$$

Step 4: Calculate V_S:
The steel contribution to shear capacity is estimated by AASHTO equation 9-30:

$$V_s = \frac{A_v f_y d}{s} = \frac{(0.40in^2)(60ksi)(25in)}{12in} = \underline{\underline{50 \text{ kips}}}$$

Step 5: Solve for the nominal shear strength by AASHTO equation 9-26:

$$V_n = V_{cw} + V_s = \underline{\underline{154 \text{ kips}}}$$

Figure 4.3: Example of Shear Capacity Calculation using AASHTO 1996

4.3.3 Flexural Capacity

The flexural capacity of the box beam was evaluated following the same AASHTO guidelines used for estimating shear strength. In addition to this calculation, a moment-curvature analysis was performed for additional insight into the flexural behavior of the box beams. The following analyses utilized a cross section perpendicular to the longitudinal axis of the beam, as shown in Figure 2.3.

4.3.3.1 Estimation of Flexural Capacity According to AASHTO Code

Estimation of the flexural capacity of the box beam was not complicated by the difficulties encountered in calculation of shear capacity. Flexure was considered in a region away from the solid, end diaphragm where geometric irregularities and debonded strands did not exist.

AASHTO Section 9.17 governs calculation of flexural strength of prestressed concrete members, and Equation 9-13 was used to calculate flexural strength. The equation is based on the equivalent rectangular stress block traditionally used in design. Using a concrete strength of 6500 psi and an average stress in the prestressing steel at ultimate strength (f^*_{su}) of 249.2 ksi (calculated using Equation 9-17), the flexural capacity was computed to be 1759 ft-kips.

4.3.3.2 Moment-Curvature Analysis

This analysis was intended to provide an estimate of ultimate flexural capacity, based on strain compatibility analysis, and to demonstrate the overall flexural behavior from initial loading to ultimate capacity.

The analysis follows the procedure used by Lin and Burns [4]. The assumptions for concrete strength and prestress loss used earlier remain the same here, but material models used in the analysis by Lin and Burns were also utilized. Based on first flexural cracking at a stress equal to $f_r = 7.5\sqrt{f_c'}$, a moment of 1222 ft-kips was calculated. For a top fiber strain of 0.003 (assumed crushing strain), the ultimate capacity was calculated to be 1870 ft-kips. Figure 4.4 shows the moment-curvature relationship for the box beam.

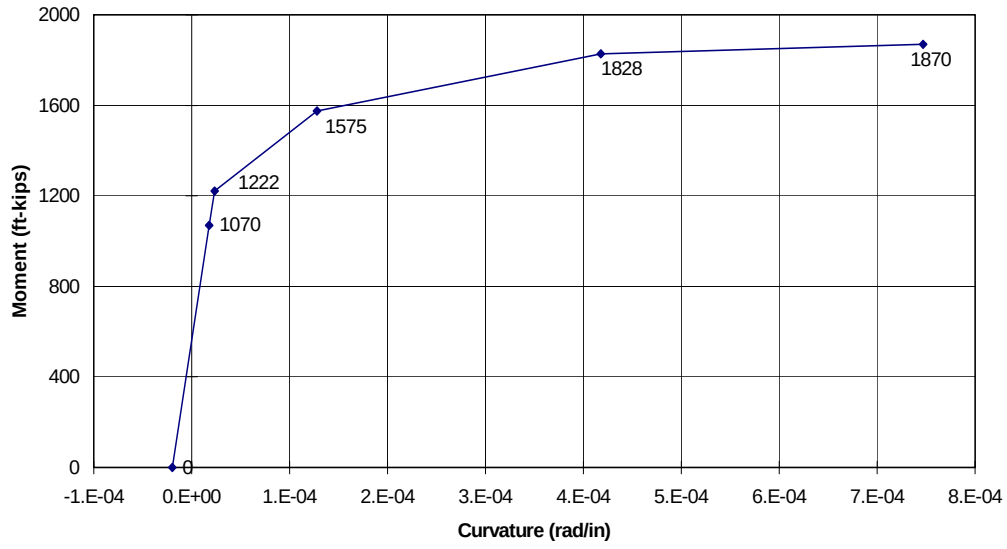

Figure 4.4: Moment-Curvature Analysis for Box Beam

4.3.4 Comparison of Calculated and Required Capacities

Results of the computations described in the previous sections are summarized in Table 4.3. Both of the analyses for the AASHTO 1996 Standard Specification for Highway Bridges for effective and completely ineffective box beam interaction are compared with capacities calculated according to AASHTO and the flexural capacity from the moment-curvature analysis. The calculated nominal shear capacity was found to be adequate compared with required capacities, even when the overload case resulting from completely ineffective box beam interaction was considered. The computed nominal capacity was 20% greater than the required strength for this case. Nominal flexural capacity compared according to AASHTO capacity, however, was exceeded by 6% for the case lacking interaction of the beams. Moment capacity calculated by strain-compatibility analysis was approximately equal to the AASHTO required capacity for the case of no beam interaction.

Table 4.3: Summary of Estimated and Required Capacities

	STANDARD AASHTO 1996	STANDARD AASHTO 1996	Calculated Nominal Capacities	
	Adequate Box Beam Interaction	Lack of Box Beam Interaction	STANDARD AASHTO 1996	Moment-Curvature Analysis
V_{TOT}	98.8 kips	127.6 kips	154 kips	
M_{TOT}	1445 ft-kips	1866 ft-kips	1759 ft-kips	1870 ft-kips

4.4 EVALUATION OF MEASURED CAPACITY AND FAILURE MODE - TEST 1

This box beam resisted a maximum applied load of 175 kips. Based on the approximations discussed in Section 4.2, the maximum shear and moment experienced by the beam were approximately 131 kips and 1000 ft-kips, respectively. The moment and shear diagrams at ultimate applied load are shown in Figure 4.5.

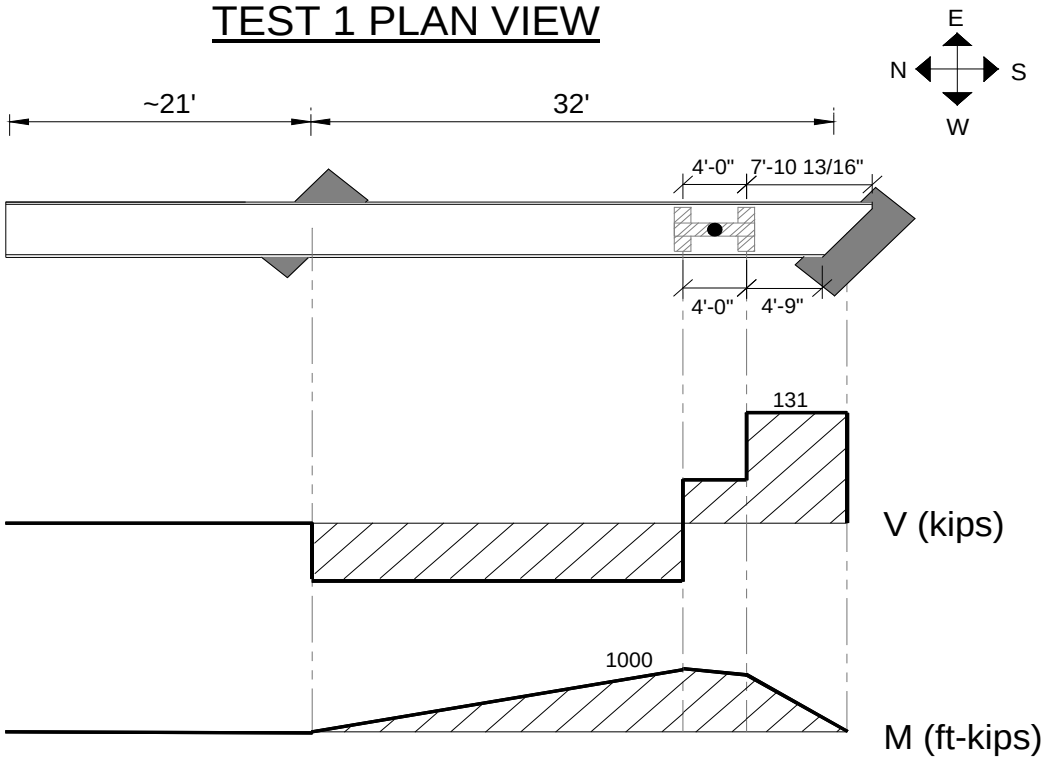

Figure 4.5: Moment and Shear Diagrams at Ultimate Load - Test 1

The maximum moment achieved was well within the elastic range, as indicated by the moment-curvature analysis (see Figure 4.4). Coincidentally, virtually no flexural cracks were observed during testing of this beam. Because a flexural failure did not occur, comparisons with computed nominal flexural capacities revealed little about the methods used to compute those capacities.

The maximum shear achieved did not reach the level predicted by the AASHTO Specification, but did exceed the required capacities for both assumptions of either adequate or inadequate box beam interaction. Cracking in the bottom flange and related strand slip very likely influenced the shear capacity.

Test results reported in Chapter Three indicated the beam failed when crushing occurred in the West web of the girder. Failure was accompanied by substantial strand slip at the end of the girder. This suggests that failure may have occurred when shear capacity was reduced as the result of loss of prestress force because of slip. Slip of the strands was likely influenced by existing cracks in the bottom flange as well as cracks that propagated during testing.

Much of the applied load during this test was directed from the nearest point of load application to the near support on the West side of the beam. Because failure appeared to precipitate in the West web, it is possible that the shear strength model may overestimate strength because the strengths of the two webs were not reached simultaneously.

4.5 EVALUATION OF MEASURED CAPACITY AND FAILURE MODE - TEST 2

An ultimate applied load of nearly 232 kips was applied during this test. Maximum moment and shear values of 1590 ft-kips and 147 kips, respectively, were computed for the loading at ultimate. Figure 4.6 shows the shear and moment diagrams for the ultimate applied loading.

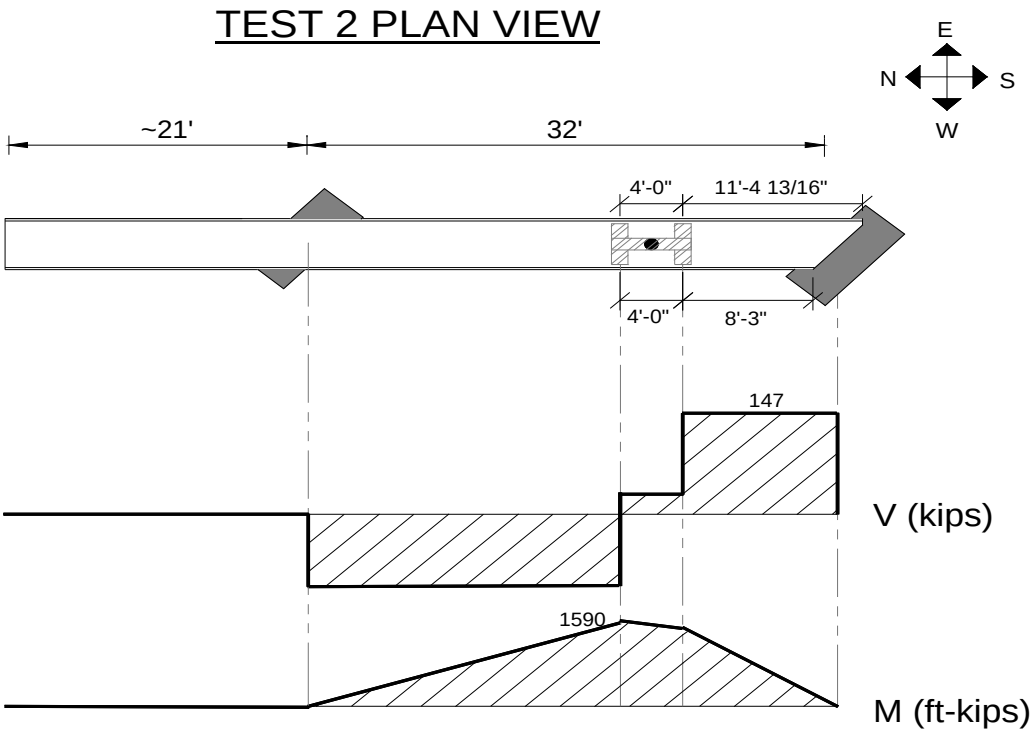

Figure 4.6: Moment and Shear Diagrams at Ultimate Load - Test 2

The maximum moment attained during this test was substantially higher than during the previous test. Flexural cracking propagated quite heavily in the region surrounding the load point. The first flexural crack, based on $f_r = 7.5\sqrt{f_c'} =$ 1222 ft-kips corresponded to an applied load of approximately 180 kips during the test, which, coincidentally was the load at which the first flexural crack was observed. This suggests that the approximate analysis used to accommodate the skewed beam end and the assumptions regarding material properties were reasonably accurate. The maximum moment reached during this test was again lower than the AASHTO projected capacity; but flexural behavior was not responsible for failure of the beam.

The maximum shear attained during this test was also higher than during the previous test. The 147-kip maximum was close to the predicted AASHTO capacity of 154 kips. Strand slip again may have played a role in decreasing the overall shear capacity as a result of reduced prestress force because of strand slip. As was reported for the previous test, the level of shear reached in this test exceeded both analyses for required shear capacity.

Web-shear cracks, flexure-shear cracks, and flexural cracks all propagated into existing cracks along the bottom of the beam. Original cracks in the bottom flange were also observed to propagate and widen.

As for the previous test, the skewed end likely resulted in shear strength being mobilized in the West web (with the shorter shear span) before it could be reached in the East web. The sum of the two shears resisted by the webs when failure precipitated in the West web should likely be less than the predicted capacity that assumed strength of the two webs being mobilized simultaneously.

Shear Capacity Estimate:

- The shear capacity at the interface of the solid end diaphragm and the hollow, box section will be calculated. The concrete contribution to shear capacity will be estimated by AASHTO equation 9-29 shown here:

$$V_{cw} = \left[\frac{3.5\sqrt{f_c'}}{1000} + 0.3f_{pc} \right] b'd$$

Section Properties:

b'=	10 inches (summation of two webs)	f_C'=	6500 psi (assumed)
d=	25 inches	f_s'=	270 ksi (TEXDOT plans)
A=	679.375 in^2 (hollow, box section)	fse=	162 ksi (0.6*fpu)

Step 1: Summation of Fse (following AASHTO Section 9.20.2.4):
Of the total 24 prestressing strands, 5 fully bonded strands have completely developed, 5 fully bonded strands are partially developed, and all 6, two foot unbonded strands are partially developed. All 8, four and six foot unbonded strands are still unbonded at this cross section.

A summation of the prestress forces at this section gives: Fse= 300.72 kips

Step 2: Calculation of f_{PC}:

$$f_{PC} = \frac{F_{SE}}{A} = \frac{300.72}{679.375} = \underline{\underline{0.433 \text{ ksi}}}$$

Step 3: Calculate V_{CW}:

$$V_{cw} = \left[\frac{3.5\sqrt{6500}}{1000} + (0.3)(0.433) \right](10)(25) = \underline{\underline{103.8 \text{ kips}}}$$

Step 4: Calculate V_S:
The steel contribution to shear capacity will be estimated by AASHTO equation 9-30 shown here:

$$V_s = \frac{A_v f_y d}{s} = \frac{(0.4\text{in}^2)(60\text{ksi})(25\text{in})}{12\text{in}} = \underline{\underline{50 \text{ kips}}}$$

Step 5: Solve for the nominal shear strength by AASHTO equation 9-26:

$$V_n = V_{cw} + V_s = \underline{\underline{153.8 \text{ kips}}}$$

CHAPTER FIVE:

ASSESSMENT OF BOX BEAM REINFORCEMENT DETAILS

5.1 INTRODUCTION

The previous chapter was concerned with strengths measured during the tests. This chapter will examine longitudinal cracking patterns that were observed before or during the tests. Observations from each test, as they relate to the pattern and location of cracking, and speculation about the cause of cracking are presented. TxDOT original and current detailing standards will then be assessed. Correlation between detailing standards and observed cracking will be drawn in order to provide a recommendation for improved detailing requirements. Additional reinforcement in end diaphragms is proposed for determining the amount and location of reinforcement. The box beams tested in this study are detailed accordingly.

5.2 OBSERVATIONS FROM TESTS

Cracking along the underside of the beam was briefly discussed in Chapters Three and Four in relation to their possible role in the failure of the beams. The previous discussions have not included explanations for why these

cracks occurred. This section will attempt to provide an explanation for the cracking observed prior to testing. Observations related to bottom-flange cracks from each test will briefly be revisited here, emphasizing similarities between cracks in different box beams.

Longitudinal cracking was observed in both girders before and after each test; Appendix D presents these crack patterns for each girder. Box Beam 3 (Test 1) contained more longitudinal cracking than Box Beam 5 (Test 2) prior to testing, but Box Beam 5 generated more of these cracks during testing. Most of the cracks observed in the bottom flange from Test 1 were from shear-flexure cracks that propagated into the bottom flange from the West web. This was not the case in Test 2 where longitudinal cracking in the bottom flange was observed to both propagate from existing cracks and form as new cracks.

Many of the longitudinal cracks appear to be common to many girders. Typical patterns and similarities between girders can be observed by closely examining the crack maps in Appendix D. The most striking similarity is the large number of diagonal cracks that propagated from the center of the bottom flange toward the edges. This pattern typically begins within two feet of the end face of the box beam, and extends diagonally out towards the edges of the beam, more than seven feet from the beam end in some cases. The second notable similarity is the purely longitudinal crack along the beam centerline. Although not observed in the untested end of Box Beam 5, many other beams displayed a crack propagating from the origin of the diagonal cracks and extending along the beam centerline for more than seven feet into the beam. The third common crack was observed approximately two feet from the end face and propagated parallel to

the skewed end. The tested end of Box Beam 5 did not exhibit this crack, but the three other beam ends mapped in Appendix D did.

Each of these crack types appeared to originate in a mass of concrete within the first two feet of the girder and in the middle third of the cross section. Possible causes include deficient mild (non-prestressed) reinforcement in the end diaphragm, debonded prestressed strands in the end diaphragm, and concrete shrinkage. Each of the above could affect the tensile stresses in the bottom flange causing cracking in the region. On the basis of the observed cracking patterns and the observed strand slip at failure in each test, the longitudinal cracking patterns were believed to be related to the strand debonding pattern used in the end diaphragms.

Examination of the location and distribution of bonded and debonded strands, as well as the non-prestressed reinforcement in the central portion of the end diaphragm provides a hint of insight into understanding the cracking behavior. All of the debonded strands were located in the interior of the section, while strands that were fully-bonded were grouped near or within the webs of the beam, as displayed earlier in Figure 2.5. The first two feet of the central, lower half of the diaphragm, which contained most of the debonded strands, contained virtually no mild reinforcement in the longitudinal direction. This relatively unreinforced region is a prime candidate for some form of cracking, and does correspond with the location of where the different crack types are believed to have originated. Some of the longitudinal cracks appear to follow the path of debonded strands. In addition, the strand debonding pattern also appears to impart a staggered precompression force pattern into the bottom flange that is

applied first beneath the web regions and applied last to the region furthest from the girder end. As a result, this lower, control region in the end diaphragm receives the least (practically no) benefit, in the form of precompression stresses, from the prestressing force.

5.3 TxDOT BOX BEAM STANDARD DETAILING

Detailing used in the box beams tested in this program was investigated and compared to current detailing procedures used by TxDOT. The purpose of this section is to determine if detailing deficiencies existed in the test beams. Focus will be on the arrangement of bonded and debonded prestressed strands and on nonprestressed reinforcement in the end diaphragm. The original plans were drawn using Imperial units, and the current standards contain SI units. In order to avoid confusion, and because this report has used Imperial units throughout, soft conversions of current details will be made.

The Final 1974 Plans from TxDOT for the Hicks Road Overpass [5] were used in this investigation. Sheets 173 and 174 detail the prestressed concrete box beam unit. Most of the detailing for bonded and debonded steel, as well as transverse reinforcement, was explained earlier in Section 2.2.3. The distribution of bonded reinforcement was shown in Figure 2.5, and transverse reinforcement is presented in Appendix A. These details, except for the distribution of debonded strands, can be found in TxDOT plans. The only note in TxDOT plans related to

debonding of strands was, "Strands with shorter bond breakage are symmetric about centerline in Row A (bottom row)."

Current detailing procedures from the TEXDOT Design Division include sheets for several box-beam configurations [6]. Two sheets labeled, Prestressed Concrete Box Beam Details BB28-1210 (4B28), closely resemble the beams tested in this program. Transverse reinforcement includes a variety of confinement steel that is very similar to that used in the test beams. Number 4 instead of the #5 bars used previously provide reinforcement in three rows parallel to the skewed end section, and spacing of these bars begins 2 inches from the beam end with two successive spacings of 6 inches. Reinforcement perpendicular to the longitudinal axis of the beam was again found to be #4 bars spaced at 6 inches within the end diaphragm. A major difference in the current standard is that this spacing extends at least 5 feet into the box section, whereas previous detailing terminated 6-inch spacing within the solid, end diaphragm. Twelve inch spacing of stirrups does exist in current detailing procedures, but does not begin until at least 5 feet from the start of the box section.

Current TxDOT detailing procedures for the distribution of debonded strands were not described in these sheets, but discussions with TxDOT design engineers indicated that current procedures call for alternating bonded and debonded strands across the section. The amount and location of prestressing strands are contingent upon each design, and therefore cannot be specified more specifically than stated above. It is not clear whether TxDOT specifies the location of each debonded strand or whether that decision is left to the precast manufacturer.

The number of debonded strands in any prestressed design are determined based on the permissible tensile stresses in the top fiber of the beam at the time of release. Because of the particularly large number of debonded strands near the end of the beam, no longitudinally-oriented, bonded reinforcement existed to intersect and control any of the cracks described previously. This deficiency was not accounted for in the original design and may or may not (depending on distribution of bonded and debonded strands) be accounted for in current designs.

5.4 RECOMMENDATIONS FOR IMPROVED BOX BEAM REINFORCEMENT DETAILS

As mentioned above, some bonded longitudinal reinforcement must be available in the bottom flange to intersect and control tensile cracks. The box beams investigated in this study contained most of the debonded strands in the central portion of the bottom flange and diaphragm where virtually no mild longitudinal reinforcement was provided. However, even a better distribution of these debonded strands may not eliminate the cracking observed in these beams. Because increasing the amount of bonded, prestressed reinforcement is not an option, a modest addition of strategically-located mild reinforcement is needed.

Supplementary tie reinforcement, commonly referred to as hairpins, should be placed along the top of debonded prestressing strands in the end diaphragm. This reinforcement will not affect prestressing or significantly affect the economy of the beams, but will provide critical, bonded steel within the weak region identified earlier. In addition, the quantity of steel to be placed is

relatively small and will not congest the end diaphragm making concrete placement more difficult.

Several methods were investigated to justify the amount of steel to be placed. Temperature and shrinkage steel, as required by AASHTO Section 8.20, was investigated as well as bottom flange minimum flexural reinforcement (AASHTO Section 9.25). The effective cross section area was used for both of these calculations, and the resulting amounts of reinforcement were found to be very small (0.51 and 0.72 sq. in., respectively).

A third method was investigated in which a strut-and-tie model was developed based on a model found in CTR Research Report 1127-3F, page 172 [2]. The purpose of the strut-and-tie model was to evaluate what bottom tensile-chord force was necessary to develop the required AASHTO shear forces at varying locations near the beam end. Two locations for the shear force were analyzed. The first was at the beginning of the box section where shear resistance is greatly reduced, and the second was two feet from the support where the maximum debonding ceased.

The first location for shear force placement produced the greatest tensile force. Figure 5.1 shows this calculation and the calculation for the required number of hairpins. Number 4 bars are used because their diameters were similar to those of the prestressing strand. Each #4 bar forms a long, slender U-shape with the bottom of the U at the end of the beam. Fourteen, #4 bar cross sections were required resulting in seven hairpins. Length was conservatively determined based on the summation of the development length of a #4 bar (AASHTO Section 8.25) and the complete development of a fully-bonded prestressed strand

(AASHTO Section 9.28). Cover over the ends of the hairpins at the beam end should be a minimum of 1 inch, as required by AASHTO Section 9.26.1.3.

Strut-and-Tie Model for Determination of Hairpin Steel:

- A model similar to Example 4.1 in CTR Research Report 1127-3F was used to evaluate the tensile force in the bottom flange necessary to develop the required AASHTO shear capacity.
- The maximum required AASHTO shear capacity at the box section interface and the properties of the section are listed below:

V_u =	115.3 kips	(factored AASHTO required shear strength)
ϕ =	0.9	(strength capacity reduction factor)
$V_n=V_u/\phi$=	128.1 kips	(nominal shear strength)
x =	3'-$^1/_2$"	(distance from support to applied shear)
CGS =	3.25 inches	(center of gravity of effective prestress steel)
d =	24.75 inches	(distance from top concrete fiber to CGS)
z ≈0.9d ≈	1.85 feet	(dist. from centriod of comp. chord to CGS)

- A partial diagram of the applied load is shown below with the strut-and-tie model below it.

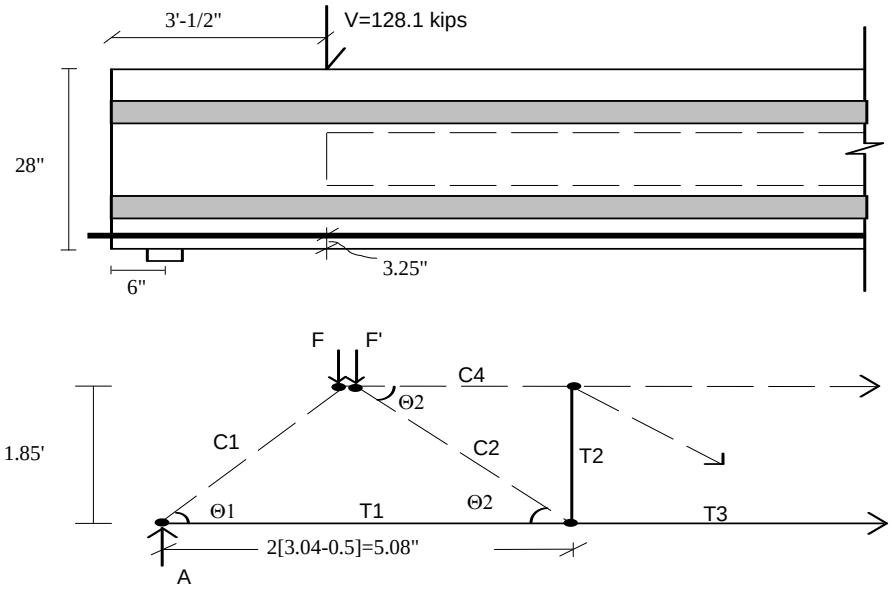

(continued on the next page)

Figure 5.1: Strut-and-Tie Model for Determination of Hairpin Steel

- The tensile chord, T1, is the tensile force from which hairpin steel shall be determined. The following calculations solve for T1:

$$A = \frac{F(L - x)}{L} = \frac{128.1(65 - 3.04)}{65} = \underline{122.1 \text{ kips}}$$

$$F = A = \underline{122.1 \text{ kips}}$$

$$\therefore F' = 128.1 - 122.1 = \underline{6.0 \text{ kips}}$$

$$\Theta 1 = \tan^{-1}\left[\frac{d}{x - 6 \text{ in.}}\right] = \tan^{-1}\left[\frac{1.85 \text{ in.}}{2.54 \text{ in.}}\right] = \underline{36.1^\circ}$$

$$T1 = \frac{F}{\tan \Theta 1} = \frac{122.1 \text{ kips}}{\tan 36.1^\circ} = \underline{167.4 \text{ kips}}$$

$$A_{s(req'd)} = \frac{T1}{f_y} = \frac{167.4 \text{ kips}}{60 \text{ ksi}} = \underline{2.79 \text{ in}^2}$$

$$\#4 \text{ bar}_{(req'd)} = \frac{2.79 \text{ in}^2}{0.2 \text{ in}^2} = 14 \Rightarrow \therefore \underline{\underline{7 \text{ hairpins required.}}}$$

- The required length of each leg of a hairpin is based on:

AASHTO Section 8.25:	#4 bar development length =	12 inches
AASHTO Section 9.28:	0.5"ϕ strand development length =	70.6 inches

Total leg length = $12 + 70.6 \approx \underline{83 \text{ inches} \approx 7 \text{ feet}}$

Figure 5.1(cont.'d): Strut-and-Tie Model for Determination of Hairpin Steel

Hairpins should be a simple and inexpensive way to place mild bonded reinforcement in the end diaphragm where a large number of debonded prestressed strands are grouped. Figure 5.2 shows the placement of the seven

hairpin bars required for the box beams considered in this study. Notice that placing and tying the additional hairpin steel directly above the already pretensioned strands should not hinder casting of concrete.

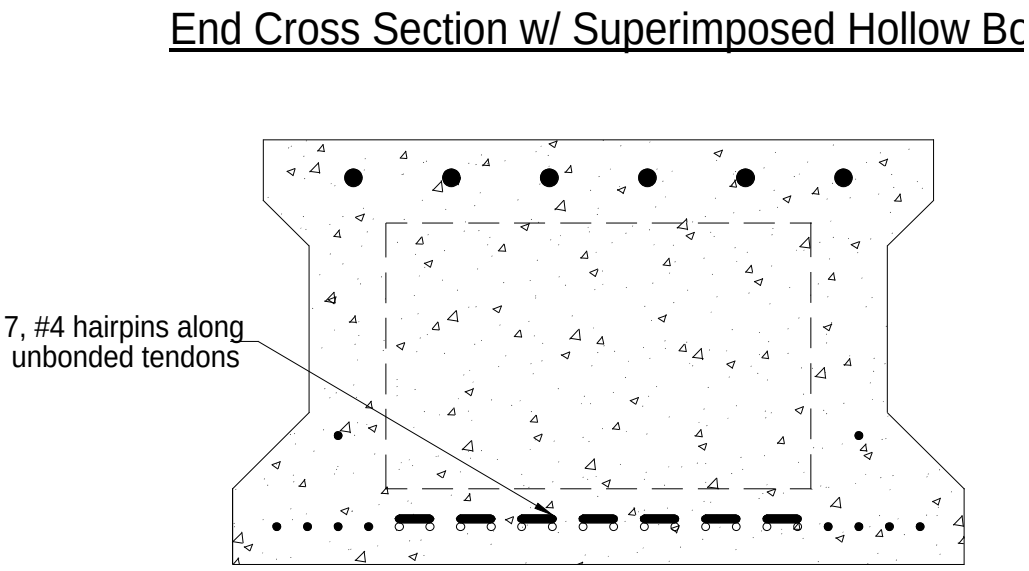

Figure 5.2: Cross-section Detailing Placement of Hairpin Steel

Strut-and-Tie Model for Determination of Hairpin Steel:

- A model similar to Example 4.1 in CTR Research Report 1127-3F will be used to evaluate the tensile force in the bottom flange necessary to develop the required AASHTO shear capacity.
- The maximum required AASHTO shear capacity at the box section interface and the properties of the section are listed below:

V_u =	115.3 kips	(factored AASHTO required shear capacity)
ϕ =	0.9	(strength capacity reduction factor)
$V_n=V_u/\phi$=	128.1 kips	(nominal shear capacity)
x =	3'-$^1/_2$"	(distance from support to applied shear)
CGS =	3.25 inches	(center of gravity of effective prestress steel)
d =	24.75 inches	(distance from top concrete fiber to CGS)
z ≈0.9d ≈	1.85 feet	(dist. from centriod of comp. chord to CGS)

- A partial diagram of the applied load is shown below with the strut-and-tie model below it.

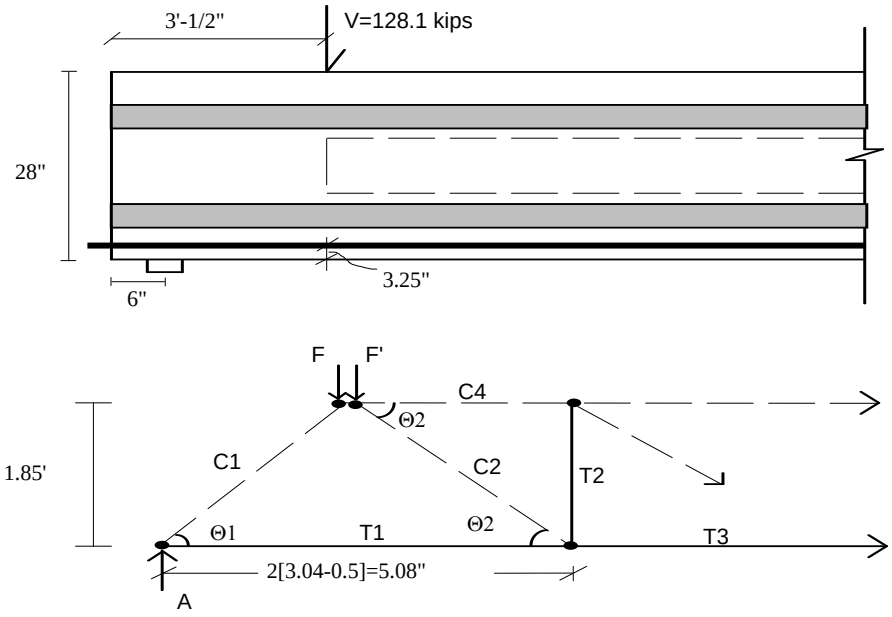

(continued on the next page)

- The tensile chord, T1, is the tensile force from which hairpin steel shall be determined. The following calculations solve for T1:

$$A = \frac{F(L - x)}{L} = \frac{128.1(65 - 3.04)}{65} = \underline{122.1 \text{ kips}}$$

$$F = A = \underline{122.1 \text{ kips}}$$

$$\therefore F' = 128.1 - 122.1 = \underline{6.0 \text{ kips}}$$

$$\Theta 1 = \tan^{-1}\left[\frac{d}{x - 6 \text{ in.}}\right] \tan^{-1}\left[\frac{1.85 \text{ in.}}{2.54 \text{ in.}}\right] = \underline{36.1^{\circ}}$$

$$T1 = \frac{F}{\tan \Theta 1} = \frac{122.1 \text{ kips}}{\tan 36.1^{\circ}} = \underline{167.4 \text{ kips}}$$

$$A_{s(req'd)} = \frac{T1}{f_y} = \frac{167.4 \text{ kips}}{60 \text{ ksi}} = \underline{2.79 \text{ in}^2}$$

$$\#4 \text{ bar}_{(req'd)} = \frac{2.79 \text{ in}^2}{0.2 \text{ in}^2} = 14 \Rightarrow \underline{\underline{\therefore \text{ 7 hairpins required.}}}$$

- The required length of each leg of a hairpin is based on:

AASHTO 8.25:	#4 bar development length =	12 inches
AASHTO 9.28:	0.5"ϕ strand =	70.6 inches

Total leg length = 12 + 70.6 ≈ <u>83 inches</u>

CHAPTER SIX: SUMMARY AND CONCLUSIONS

6.1 SUMMARY

This study investigated the irregular cracking patterns that occurred in the bottom flanges of prestressed concrete box beams from the Hicks Road Overpass on U.S. Highway 287 in Tarrant County near Fort Worth, Texas. This cracking occurred at the ends of girders, and typically originated within two feet of the end face of the beam. Typical crack patterns consisted of longitudinal cracks that propagated diagonally from the central portion of the bottom flange toward the girder webs. Close monitoring of the cracks by TxDOT engineers revealed crack growth was occurring with time. Because the mechanism for these cracks was not known, and because cracking continued to progress with time, TxDOT officials decided to test two of the girders to ascertain the current strength of the girders and to determine the cause of cracking. This information was pertinent to similar bridges in Texas that have also experienced similar cracking.

The bridge was disassembled in June, 1996, and two of the 65-foot girders were shipped to Ferguson Structural Engineering Laboratory at The University of Texas at Austin for testing. Two tests were performed in April 1997 and the results are reported in this thesis. Test 1 had a shorter shear span and smaller ultimate applied load and shear than Test 2. Correct prediction of first flexural cracking in the second test demonstrated that several assumptions made in the

beam analysis and with respect to material properties were valid. The second test also produced cracking in the beam bottom flange similar to that which was observed in the field. Both tests demonstrated shear capacities that were greater than required by the AASHTO Design Specifications, even when overload scenarios due to lack of composite action by beams were considered.

Conclusions were drawn related to the cause of cracking in the girders, and a recommendation for additional detail reinforcement was made to control cracking in the bottom flange near the ends of pretensioned box girders.

6.2 CONCLUSIONS

The following conclusions were drawn from field data, test data, evaluation of crack patterns, and evaluation of TxDOT detailing standards:

1. Observations in the field of separation of box girders coupled with bottom flange cracking and limited shear cracks suggest that transverse post-tensioned strands were not successful in making the box girders act compositely, and indicate that the box beams were subjected to loads exceeding original design loads.
2. Results of shear tests compared with current AASHTO-required capacities indicated that the capacity of the box beams in their current state was adequate, even when overloads due to complete lack of composite action between girders was considered.

3. In each test, shear failure of the girders was accompanied by dramatic slip of the debonded strands.
4. Cracking in the bottom flange was believed to originate in the central third of the diaphragm which contained little bonded reinforcement (virtually none in the longitudinal direction). Propagation of the cracks in the bottom flange likely occurred for a combination of reasons including: the relative lack of bonded steel in the central portion of the bottom flange, concentration of debonded strands in the central region of the bottom flange, and repeated overload of the girders because of a lack of composite action between girders.
5. Mild longitudinal reinforcement should be placed in locations of heavy strand debonding, as described in Section 5.4. Hairpin reinforcement placed along the unbonded prestressed strands was recommended for box beams like those from the Hicks Road Overpass. A method for determining the quantity of reinforcement was described in Section 5.4.

Appendix A

End Diaphragm Transverse Reinforcement

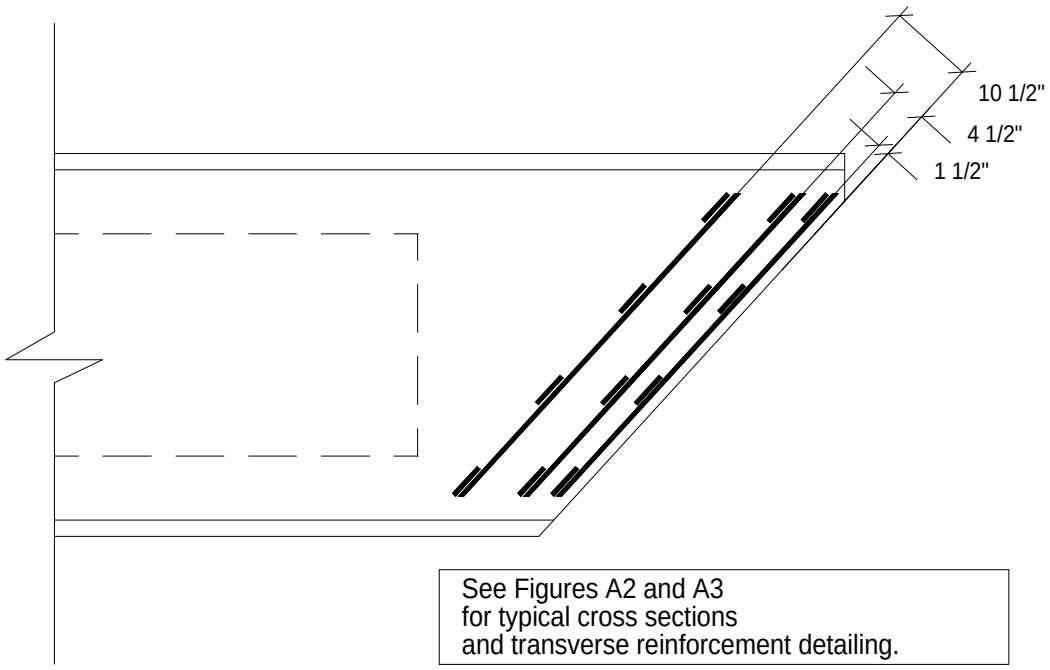

Figure A1: Plan View of Diagonal Reinforcement

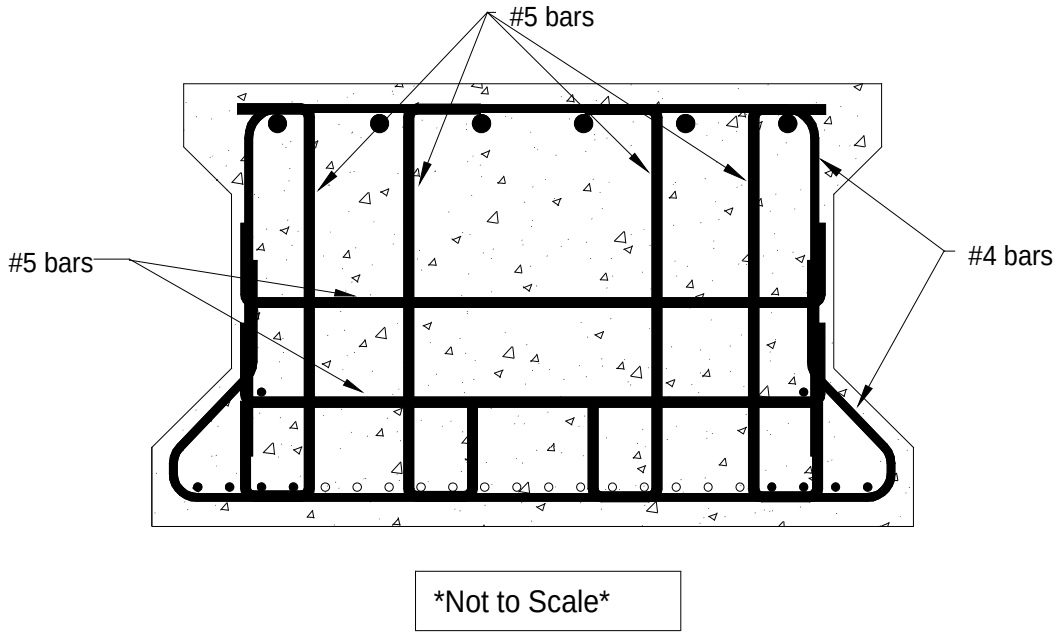

Figure A2: Diagonal Reinforcement at 1½ inches from End Face

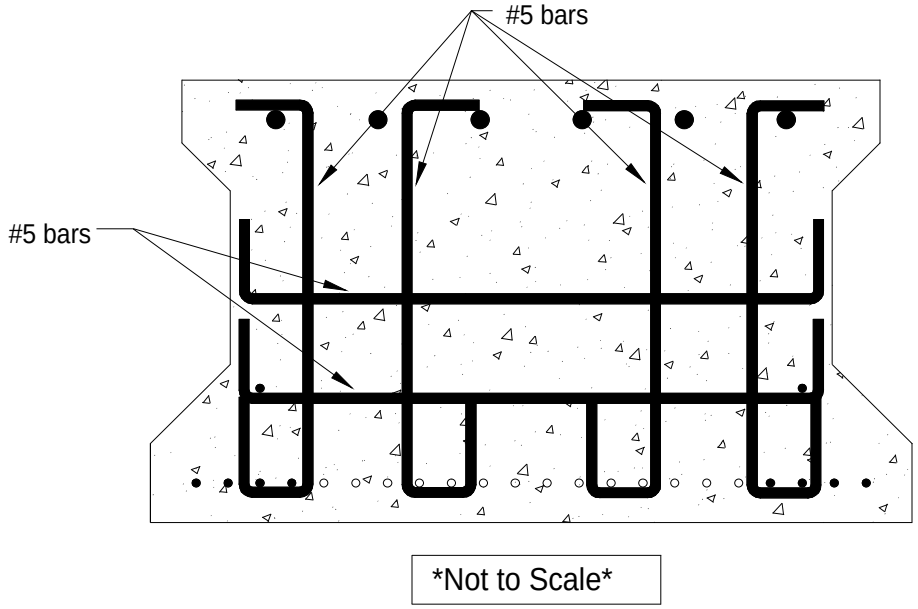

Figure A3: Diagonal Reinforcement at 4½ in. and 10½ in. from End Face

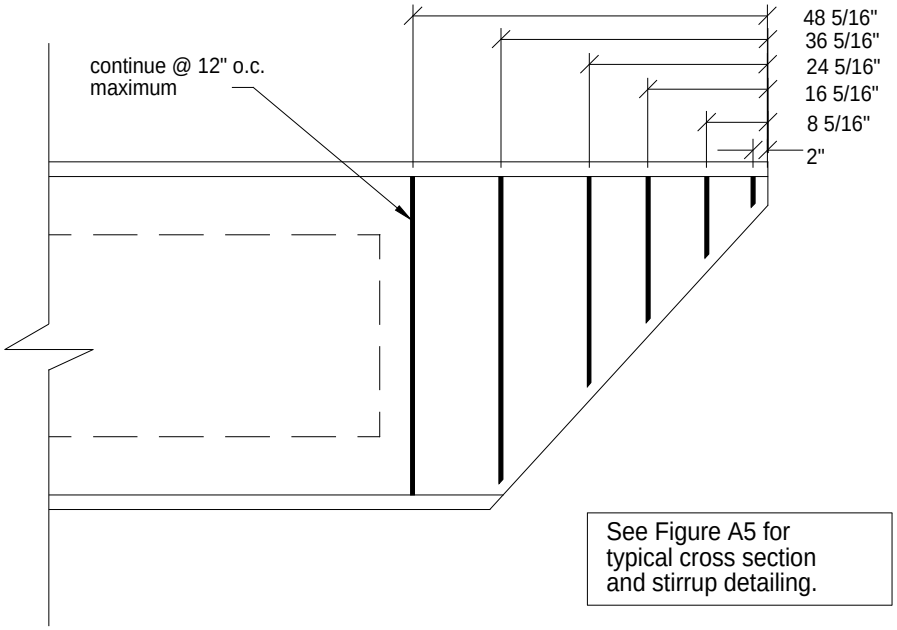

Figure A4: Plan View of Stirrups

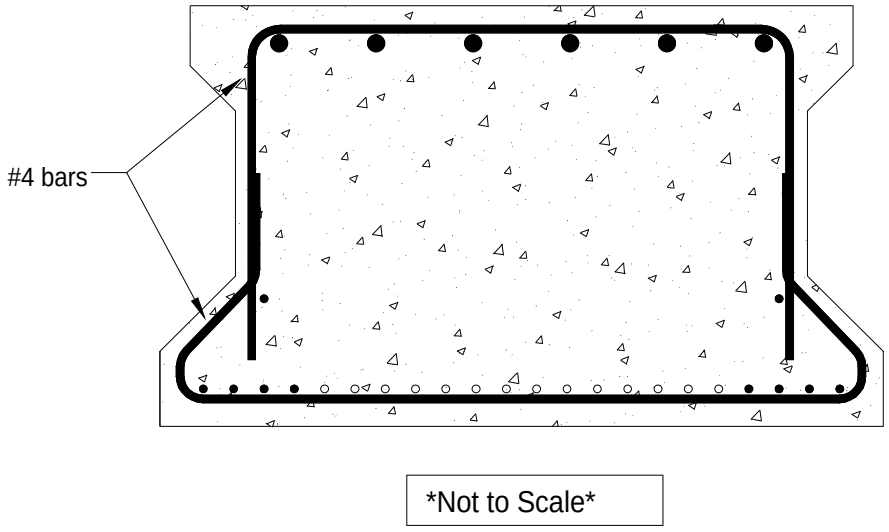

Figure A5: Typical Stirrup Reinforcement in End Diaphragm

Appendix B

Test 1 Data

Table B1: Load-Point Deflections

Applied Load	East Load-Point Deflection	West Load-Point Deflection
(kips)	(inches)	(inches)
11.340	0.052	0.061
20.931	0.093	0.113
30.522	0.126	0.153
39.714	0.161	0.191
49.755	0.193	0.230
60.246	0.227	0.268
70.388	0.257	0.302
79.829	0.281	0.328
89.621	0.310	0.359
100.912	0.337	0.387
110.703	0.364	0.413
120.145	0.388	0.439
130.386	0.413	0.465
140.777	0.441	0.493
150.820	0.468	0.520
161.059	0.495	0.546
169.354	0.524	0.574
160.261	0.530	0.580
160.611	0.546	0.589
161.860	0.565	0.600
166.007	0.583	0.616
170.403	0.629	0.659
175.398	0.680	0.706
156.515	0.697	0.722
159.061	0.742	0.763
150.768	0.748	0.773
151.817	0.803	0.831
157.263	0.851	0.883
158.460	0.909	0.953
138.378	0.934	0.979
133.532	0.946	0.994
0.049	0.347	0.377

Table B2: Bearing Pad Deflections at South Support

Applied Load	East Bearing Pad Deflection	West Bearing Pad Deflection
(kips)	(inches)	(inches)
11.340	0.039	0.058
20.931	0.068	0.100
30.522	0.088	0.129
39.714	0.108	0.157
49.755	0.127	0.184
60.246	0.146	0.210
70.388	0.161	0.229
79.829	0.173	0.245
89.621	0.188	0.263
100.912	0.199	0.281
110.703	0.209	0.294
120.145	0.219	0.310
130.386	0.229	0.327
140.777	0.238	0.342
150.820	0.248	0.359
161.059	0.257	0.375
169.354	0.266	0.392
160.261	0.269	0.405
160.611	0.272	0.418
161.860	0.274	0.429
166.007	0.276	0.440
170.403	0.281	0.494
175.398	0.293	0.574
156.515	0.292	0.593
159.061	0.296	0.646
150.768	0.300	0.671
151.817	0.309	0.743
157.263	0.316	0.801
158.460	0.330	0.882
138.378	0.339	0.946
133.532	0.340	0.968
0.049	0.143	0.457

Table B3: Bearing Pad Deflections at North Support

Applied Load	East Bearing Pad Deflection	West Bearing Pad Deflection
(kips)	(inches)	(inches)
11.340	0.015	0.016
20.931	0.027	0.031
30.522	0.039	0.044
39.714	0.052	0.057
49.755	0.066	0.069
60.246	0.081	0.083
70.388	0.095	0.094
79.829	0.107	0.101
89.621	0.121	0.111
100.912	0.136	0.121
110.703	0.149	0.132
120.145	0.162	0.141
130.386	0.186	0.150
140.777	0.190	0.159
150.820	0.203	0.170
161.059	0.216	0.182
169.354	0.229	0.187
160.261	0.233	0.186
160.611	0.235	0.188
161.860	0.238	0.190
166.007	0.245	0.194
170.403	0.256	0.197
175.398	0.265	0.200
156.515	0.268	0.204
159.061	0.272	0.206
150.768	0.274	0.208
151.817	0.276	0.210
157.263	0.277	0.211
158.460	0.285	0.214
138.378	0.283	0.217
133.532	0.285	0.218
0.049	0.000	0.000

Table B4: Strand Slip Measurements

Applied Load	End Slip Strand #1	End Slip Strand #2	End Slip Strand #3	End Slip Strand #4	End Slip Strand #5	End Slip Strand #6	End Slip Strand #7	End Slip Strand #8	End Slip Strand #9	End Slip Strand #10
(kips)	(inches)	(inches)	(inches)	(inches)	(inches)	(inches)	(inches)	(inches)	(inches)	(inches)
11.340	0.000	0.000	0.000	0.000	0.000	0.000	0.000	0.000	0.000	0.000
20.931	0.000	0.000	0.000	0.000	0.000	0.000	0.002	0.000	0.000	0.000
30.522	0.000	0.000	0.001	0.000	0.000	0.001	0.003	0.000	0.000	0.000
39.714	0.000	0.001	0.001	0.000	-0.001	0.001	0.003	0.000	0.000	0.000
49.755	0.000	0.001	0.001	0.001	-0.001	0.001	0.003	0.000	0.000	0.000
60.246	0.000	0.001	0.001	0.001	0.000	0.001	0.003	0.000	0.000	0.000
70.388	0.000	0.002	0.002	0.001	0.000	0.001	0.004	0.000	0.000	0.000
79.829	0.000	0.002	0.002	0.001	0.000	0.001	0.004	0.001	0.000	0.000
89.621	0.000	0.002	0.003	0.002	-0.007	0.001	0.004	0.001	0.000	0.000
100.912	0.000	0.004	0.003	0.003	-0.007	0.002	0.004	0.001	0.000	0.000
110.703	0.000	0.005	0.004	0.003	-0.006	0.003	0.004	0.001	0.000	0.000
120.145	0.000	0.006	0.006	0.004	-0.005	0.003	0.005	0.001	0.000	0.000
130.386	0.000	0.007	0.006	0.003	-0.004	0.003	0.005	0.001	0.000	0.000
140.777	0.000	0.008	0.008	0.005	-0.004	0.004	0.006	0.001	0.000	0.000
150.820	0.000	0.010	0.008	0.008	-0.002	0.006	0.007	0.001	0.001	0.001
161.059	0.000	0.012	0.013	0.011	0.000	0.008	0.009	0.003	0.002	0.001
169.354	0.000	0.016	0.016	0.014	0.003	0.011	0.012	0.004	0.004	0.002
160.261	0.000	0.026	0.025	0.021	0.009	0.018	0.019	0.009	0.009	0.006
160.611	0.002	0.033	0.032	0.025	0.013	0.024	0.025	0.013	0.013	0.011
161.860	0.005	0.037	0.036	0.030	0.017	0.029	0.029	0.015	0.018	0.016
166.007	0.005	0.042	0.040	0.034	0.020	0.033	0.031	0.019	0.022	0.016
170.403	0.018	0.061	0.058	0.048	0.035	0.048	0.040	0.026	0.034	0.024
175.398	0.036	0.096	0.090	0.075	0.061	0.074	0.058	0.040	0.049	0.036
156.515	0.036	0.107	0.100	0.083	0.072	0.086	0.077	0.055	0.069	0.054
159.061	0.037	0.127	0.121	0.101	0.091	0.103	0.102	0.069	0.086	0.069
150.768	0.049	0.137	0.130	0.108	0.100	0.110	0.114	0.077	0.093	0.073
151.817	0.050	0.162	0.152	0.128	0.122	0.130	0.137	0.094	0.110	0.085
157.263	0.050	0.179	0.168	0.144	0.136	0.146	0.154	0.107	0.124	0.101
158.460	0.056	0.199	0.188	0.162	0.152	0.163	0.173	0.120	0.139	0.113
138.378	0.067	0.228	0.215	0.183	0.168	0.185	0.196	0.136	0.158	0.123
133.532	0.067	0.236	0.224	0.192	0.175	0.195	0.206	0.143	0.167	0.147
0.049	0.066	0.125	0.122	0.112	0.085	0.104	0.113	0.074	0.090	0.094

Table B5: Strain Gage Measurements

Applied Load	East Strain Gage	West Strain Gage
(kips)	(in.10^{-6}/in)	(in.10^{-6}/in)
11.340	-2.9	-13.9
20.931	-5.8	-24.3
30.522	-7.8	-40.7
39.714	-11.7	-59.3
49.755	-14.6	-118.9
60.246	-17.5	-133.4
70.388	-20.4	-151.0
79.829	-25.3	-159.2
89.621	-32.1	-177.2
100.912	-38.9	-194.8
110.703	-45.6	-204.6
120.145	-51.5	-447.9
130.386	-59.3	-462.7
140.777	-68.1	-479.8
150.820	-75.7	-496.0
161.059	-86.3	-513.1
169.354	-96.7	-528.2
160.261	-87.1	-515.1
160.611	-86.1	-523.6
161.860	-88.8	-521.9
166.007	-92.6	-530.1
170.403	-93.5	-543.5
175.398	-81.9	-529.0
156.515	-74.3	-518.7
159.061	-74.2	-521.0
150.768	-61.8	-519.1
151.817	-52.3	-524.6
157.263	-54.3	-540.3
158.460	-44.7	-558.1
138.378	-20.9	-542.5
133.532	-14.2	-540.0
0.049	7.7	-352.4

Appendix C

Test 2 Data

Table C1: Load-Point Deflections

Applied Load	East Load-Point Deflection	West Load-Point Deflection
(kips)	(inches)	(inches)
11.390	0.069	0.078
20.981	0.122	0.141
30.922	0.169	0.200
40.414	0.215	0.251
51.154	0.264	0.304
61.245	0.311	0.353
70.837	0.354	0.394
81.128	0.397	0.436
90.619	0.431	0.472
100.710	0.471	0.510
110.702	0.508	0.547
120.842	0.549	0.587
131.383	0.588	0.626
141.274	0.630	0.666
150.816	0.666	0.699
161.207	0.709	0.741
170.798	0.750	0.781
180.739	0.813	0.840
190.580	0.907	0.923
200.572	1.091	1.090
210.313	1.274	1.265
206.916	1.276	1.267
216.158	1.442	1.424
219.457	1.574	1.551
221.105	1.662	1.632
225.551	1.756	1.723
220.706	1.757	1.727
227.700	1.860	1.828
231.846	1.971	1.937
230.497	2.025	2.000
142.025	2.084	2.100
0.300	0.812	0.853

Table C2: Bearing Pad Deflections at South Support

Applied Load	East Bearing Pad Deflection	West Bearing Pad Deflection
(kips)	(inches)	(inches)
11.390	0.035	0.062
20.981	0.062	0.107
30.922	0.085	0.146
40.414	0.109	0.181
51.154	0.131	0.215
61.245	0.152	0.244
70.837	0.169	0.268
81.128	0.184	0.291
90.619	0.194	0.307
100.710	0.207	0.326
110.702	0.218	0.343
120.842	0.229	0.361
131.383	0.239	0.376
141.274	0.251	0.391
150.816	0.258	0.404
161.207	0.267	0.418
170.798	0.274	0.431
180.739	0.285	0.450
190.580	0.297	0.472
200.572	0.314	0.508
210.313	0.327	0.567
206.916	0.329	0.581
216.158	0.218	0.622
219.457	0.206	0.656
221.105	0.205	0.695
225.551	0.209	0.728
220.706	0.210	0.729
227.700	0.216	0.755
231.846	0.169	0.779
230.497	0.176	0.788
142.025	0.253	0.831
0.300	0.177	0.414

Table C3: Bearing Pad Deflections at North Support

Applied Load	East Load Point Deflection	West Load Point Deflection
(kips)	(inches)	(inches)
11.390	0.069	0.078
20.981	0.122	0.141
30.922	0.169	0.200
40.414	0.215	0.251
51.154	0.264	0.304
61.245	0.311	0.353
70.837	0.354	0.394
81.128	0.397	0.436
90.619	0.431	0.472
100.710	0.471	0.510
110.702	0.508	0.547
120.842	0.549	0.587
131.383	0.588	0.626
141.274	0.630	0.666
150.816	0.666	0.699
161.207	0.709	0.741
170.798	0.750	0.781
180.739	0.813	0.840
190.580	0.907	0.923
200.572	1.091	1.090
210.313	1.274	1.265
206.916	1.276	1.267
216.158	1.442	1.424
219.457	1.574	1.551
221.105	1.662	1.632
225.551	1.756	1.723
220.706	1.757	1.727
227.700	1.860	1.828
231.846	1.971	1.937
230.497	2.025	2.000
142.025	2.084	2.100
0.300	0.812	0.853

Table C4: Strand Slip Measurements

Applied Load	End Slip Strand #1	End Slip Strand #2	End Slip Strand #3	End Slip Strand #4	End Slip Strand #5	End Slip Strand #6	End Slip Strand #7	End Slip Strand #8	End Slip Strand #9	End Slip Strand #10
(kips)	(inches)	(inches)	(inches)	(inches)	(inches)	(inches)	(inches)	(inches)	(inches)	(inches)
11.390	0.000	0.000	0.000	0.000	0.000	0.000	0.000	0.000	0.000	0.000
20.981	0.000	0.000	0.000	-0.001	0.000	0.000	0.000	0.000	0.000	0.000
30.922	0.000	0.000	0.000	-0.001	0.000	0.000	0.000	0.000	0.000	0.000
40.414	0.000	0.001	-0.001	-0.001	0.000	0.000	0.000	0.000	0.000	0.000
51.154	0.000	0.002	0.000	-0.001	0.000	0.000	0.000	0.000	0.000	0.000
61.245	0.000	0.002	0.001	0.000	0.000	0.001	0.000	0.000	0.000	0.000
70.837	0.000	0.002	0.001	0.000	0.001	0.001	0.000	0.000	0.000	0.000
81.128	0.000	0.003	0.001	0.000	0.001	0.002	0.000	0.000	0.000	0.000
90.619	0.000	0.003	0.001	0.001	0.001	0.002	0.000	0.001	0.001	0.000
100.710	0.000	0.004	0.001	0.002	0.002	0.002	0.001	0.001	0.001	0.000
110.702	0.000	0.005	0.002	0.003	0.002	0.003	0.001	0.001	0.001	0.000
120.842	0.000	0.005	0.003	0.004	0.003	0.003	0.001	0.001	0.001	0.000
131.383	0.000	0.006	0.003	0.005	0.003	0.003	0.002	0.001	0.001	0.001
141.274	0.000	0.006	0.004	0.006	0.004	0.003	0.002	0.001	0.001	0.001
150.816	0.000	0.007	0.005	0.007	0.005	0.004	0.003	0.002	0.002	0.001
161.207	0.000	0.008	0.006	0.008	0.006	0.005	0.004	0.002	0.002	0.001
170.798	0.000	0.009	0.007	0.010	0.007	0.006	0.004	0.002	0.002	0.002
180.739	0.000	0.011	0.008	0.011	0.008	0.007	0.005	0.003	0.003	0.002
190.580	0.000	0.012	0.010	0.013	0.009	0.008	0.006	0.005	0.004	0.003
200.572	0.000	0.015	0.013	0.013	0.011	0.010	0.008	0.006	0.005	0.004
210.313	0.000	0.027	0.025	0.027	0.023	0.022	0.022	0.017	0.017	0.014
206.916	0.000	0.035	0.033	0.034	0.029	0.029	0.028	0.023	0.023	0.019
216.158	0.000	0.039	0.038	0.038	0.034	0.034	0.032	0.026	0.028	0.023
219.457	0.000	0.042	0.043	0.053	0.037	0.039	0.036	0.029	0.033	0.029
221.105	0.000	0.050	0.057	0.071	0.047	0.056	0.047	0.037	0.047	0.047
225.551	0.000	0.060	0.073	0.090	0.057	0.070	0.057	0.049	0.061	0.062
220.706	0.000	0.063	0.083	0.097	0.060	0.080	0.062	0.055	0.068	0.071
227.700	0.000	0.068	0.094	0.110	0.070	0.090	0.067	0.061	0.077	0.083
231.846	0.000	0.084	0.108	0.132	0.072	0.102	0.073	0.066	0.086	0.098
230.497	0.000	0.113	0.136	0.151	0.060	0.119	0.088	0.078	0.100	0.111
142.025	-1.301	0.441	0.413	0.392	0.078	0.332	0.284	0.100	0.326	0.306
0.300	-1.301	0.311	0.296	0.251	0.045	0.211	0.235	0.114	0.225	0.196

Table C5: Strain Gage Measurements

Applied Load	East Strain Gage	West Strain Gage
(kips)	(in.10^{-6}/in)	(in.10^{-6}/in)
11.390	-5.5	-10.7
20.981	-9.2	-18.5
30.922	-13.9	-28.8
40.414	-16.6	-35.7
51.154	-22.1	-46.4
61.245	-27.5	-58.4
70.837	-32.9	-69.5
81.128	-42.2	-85.7
90.619	-51.5	-96.4
100.710	-61.8	-112.6
110.702	-72.2	-128.5
120.842	-82.4	-137.3
131.383	-94.6	-158.1
141.274	-106.6	-172.0
150.816	-118.4	-182.6
161.207	-131.4	-194.6
170.798	-146.3	-208.0
180.739	-160.2	-224.6
190.580	-171.4	-239.8
200.572	-180.7	-249.2
210.313	-200.8	-257.5
206.916	-197.0	-249.2
216.158	-209.7	-263.5
219.457	-222.3	-268.6
221.105	-226.6	-269.4
225.551	-234.2	-269.1
220.706	-228.7	-265.0
227.700	-238.9	-276.1
231.846	-245.6	-278.0
230.497	-243.7	-276.1
142.025	-117.7	-170.8
0.300	-4.0	-20.6

Appendix D

Longitudinal Crack Mapping

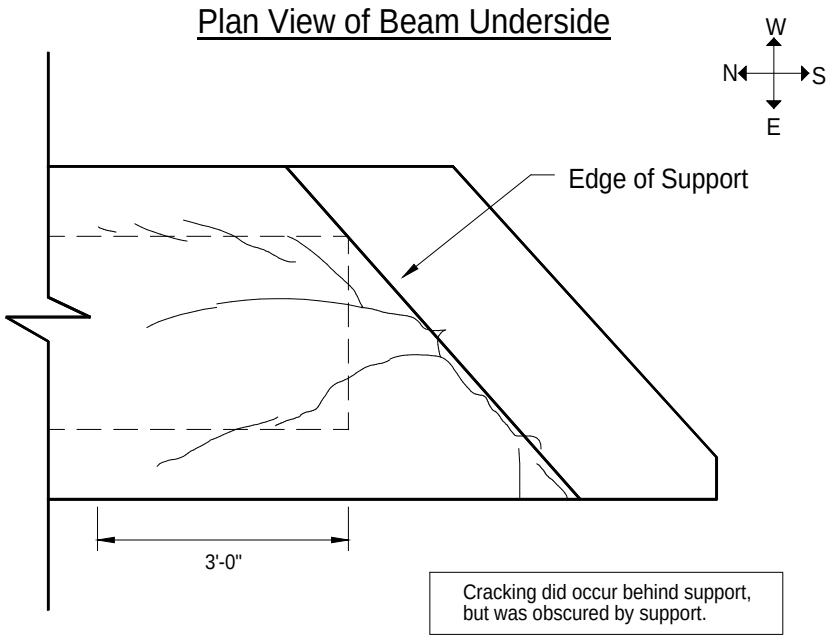

Figure D1: Pretest Cracking in Bottom Flange of Box Beam 3 - Test 1

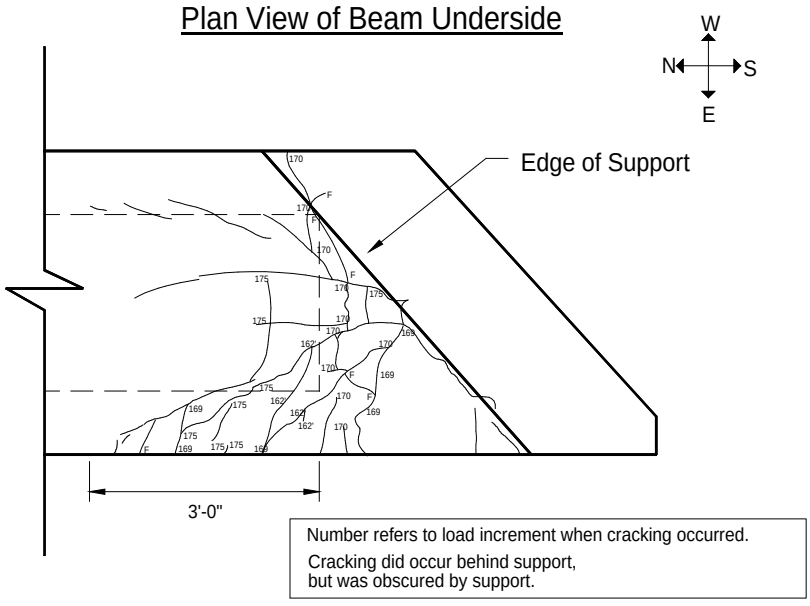

Figure D2: Post-test Cracking in Bottom Flange of Box Beam 3 - Test 1

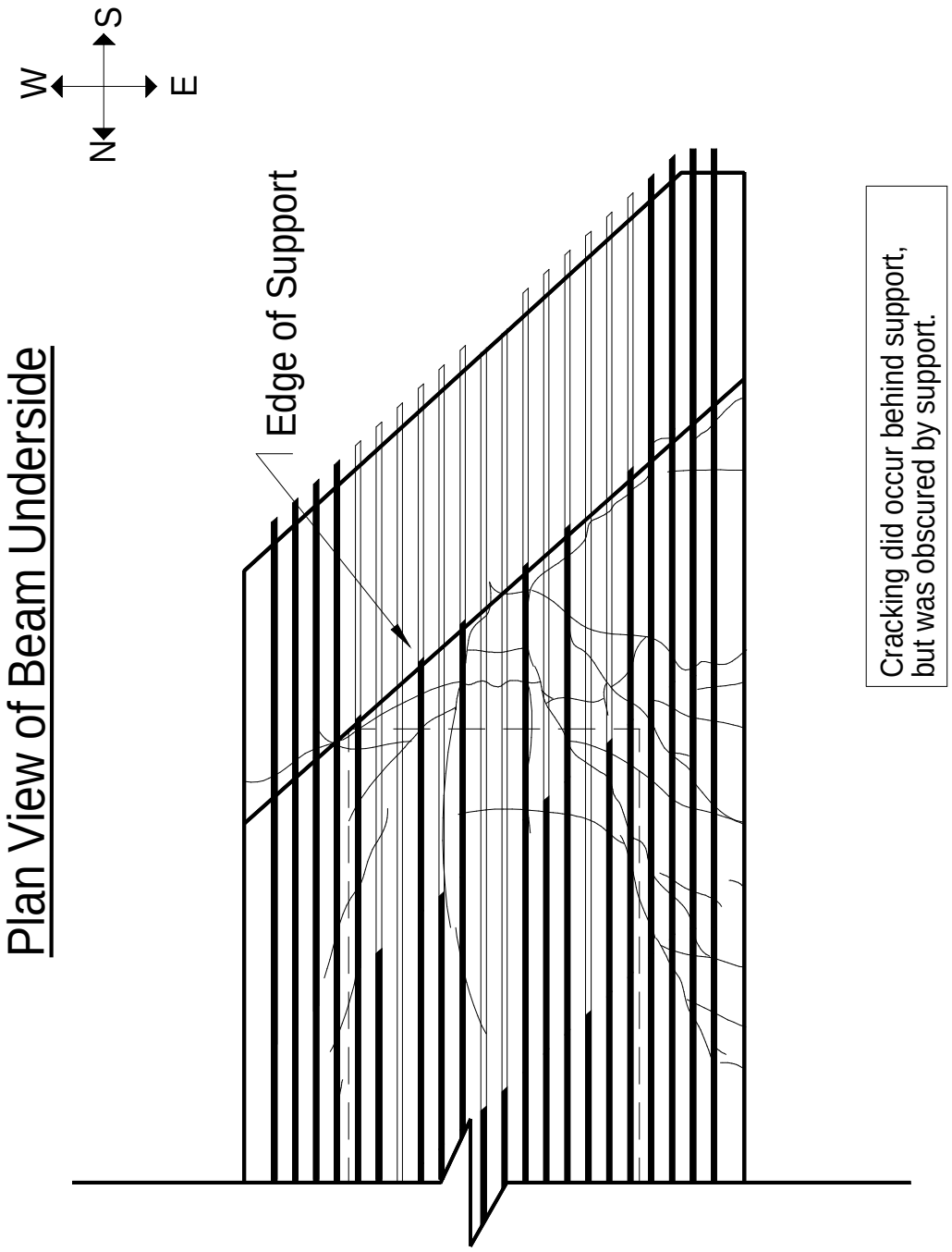

Figure D3: Post-test Cracking on Bottom Flange of Box Beam 3 - Test 1 w/ superimposed pretensioned steel

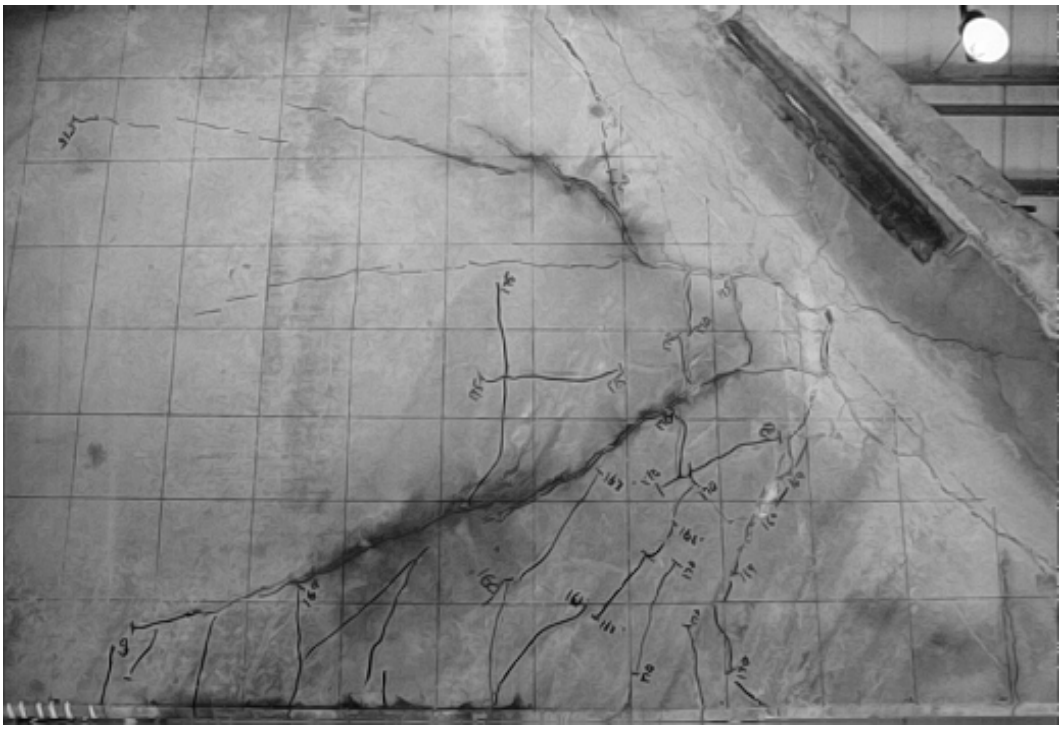

Figure D4: Photograph after Testing of Beam Underside, Box Beam 3 - Test 1

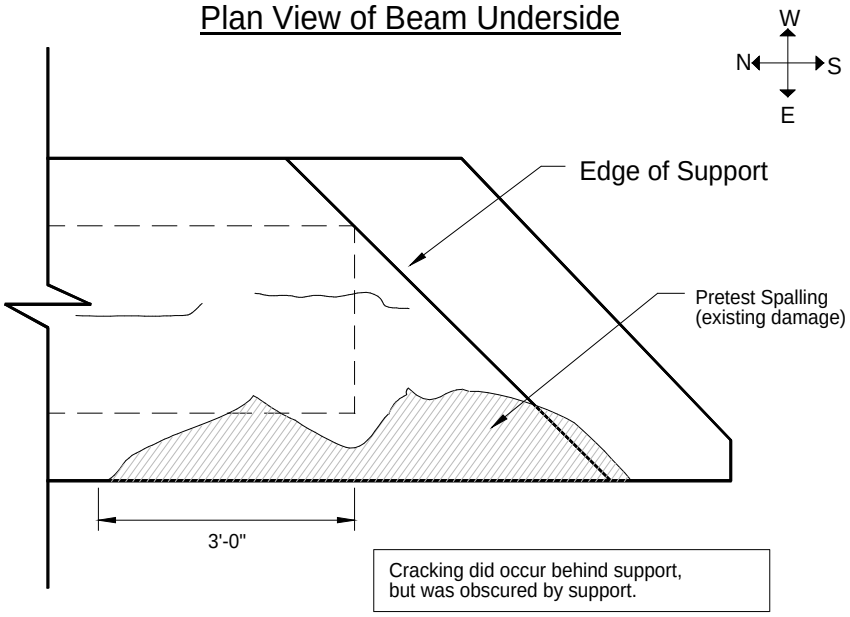

Figure D5: Pretest Cracking in Bottom Flange of Box Beam 5 - Test 2

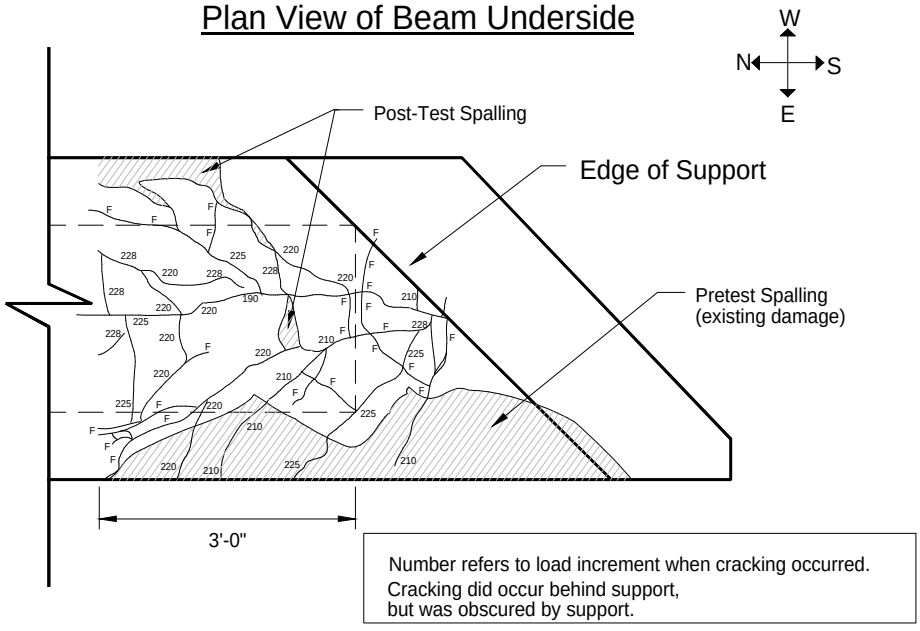

Figure D6: Post-test Cracking in Bottom Flange of Box Beam 5 - Test 2

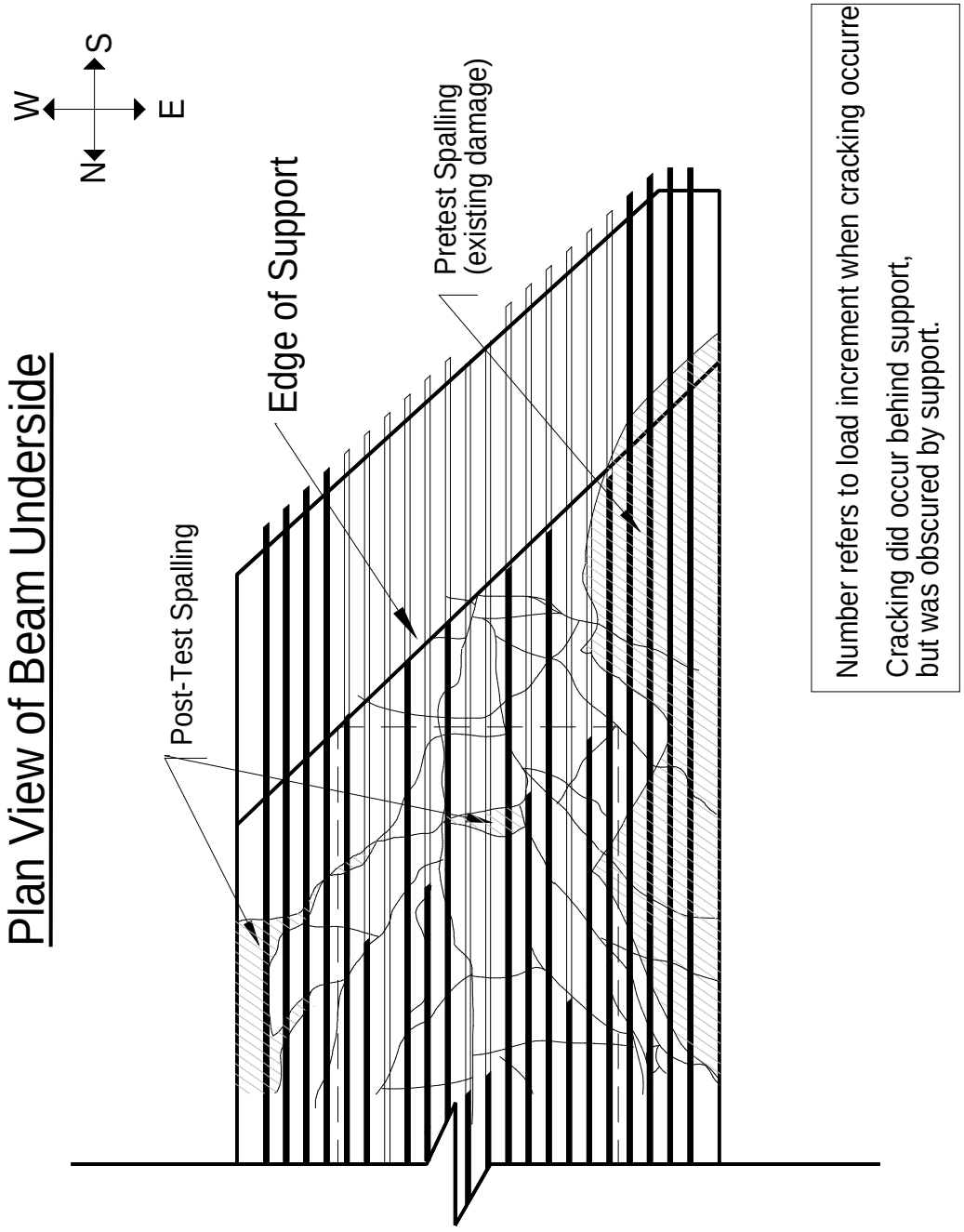

Figure D7: Post-test Cracking in Bottom Flange of Box Beam 5 - Test 2 w/ superimposed pretensioned steel

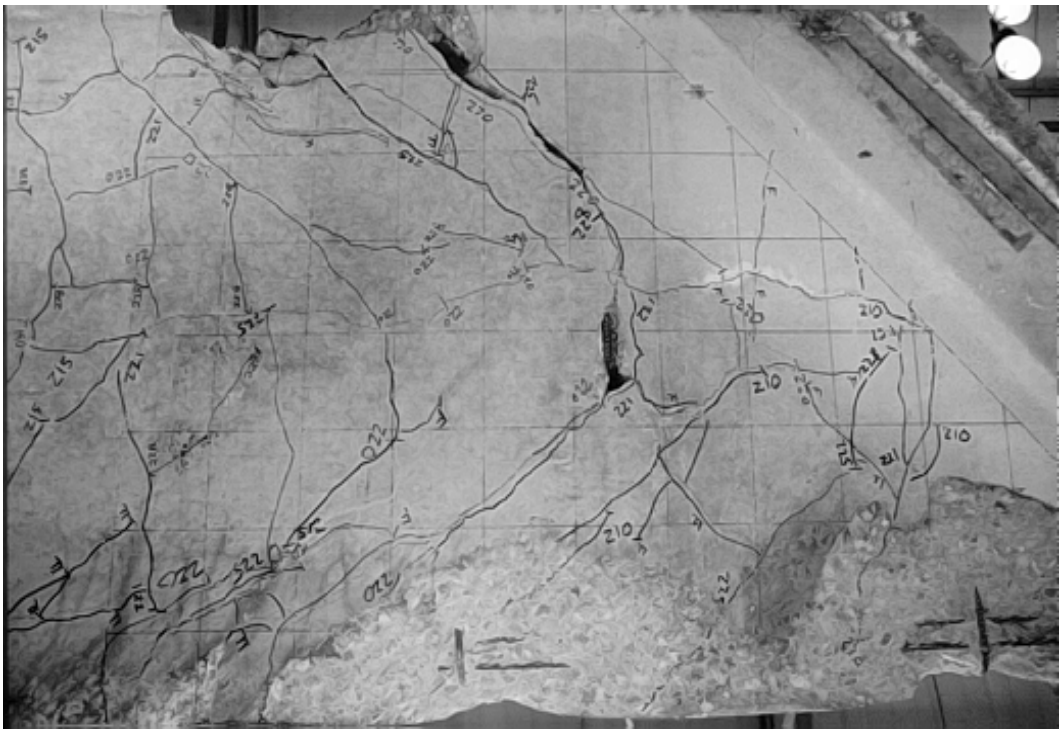

Figure D8: Photograph after Testing of Beam Underside, Box Beam 5 - Test 2

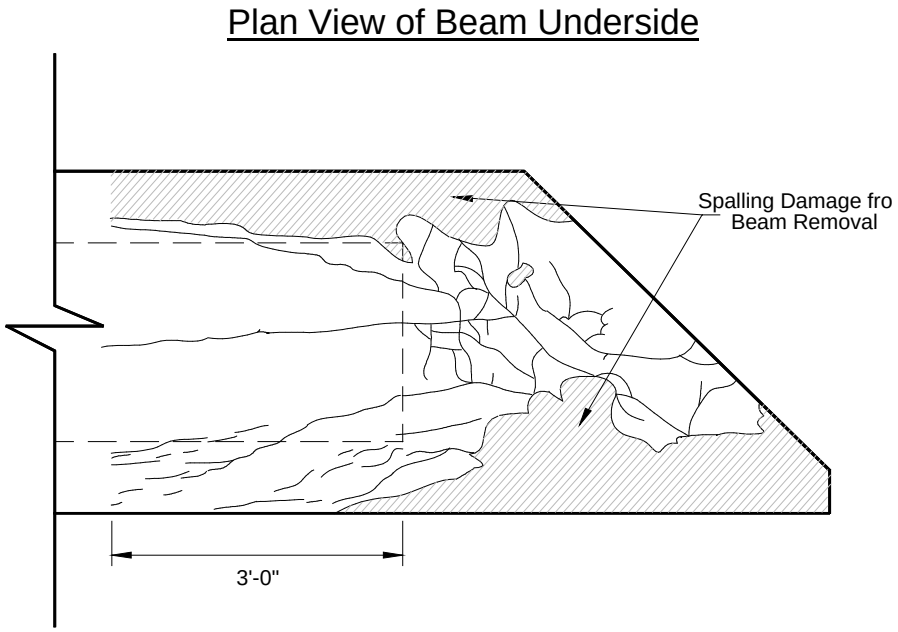

Figure D9: Cracking in Bottom Flange of Box Beam 3 - Untested End

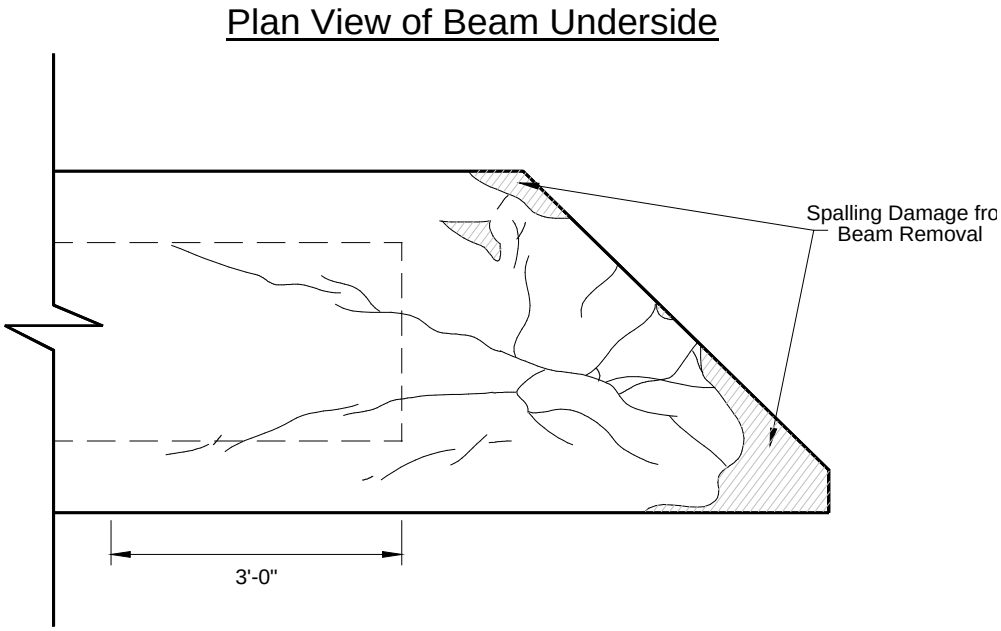

Figure D10: Cracking in Bottom Flange of Box Beam 5 - Untested End

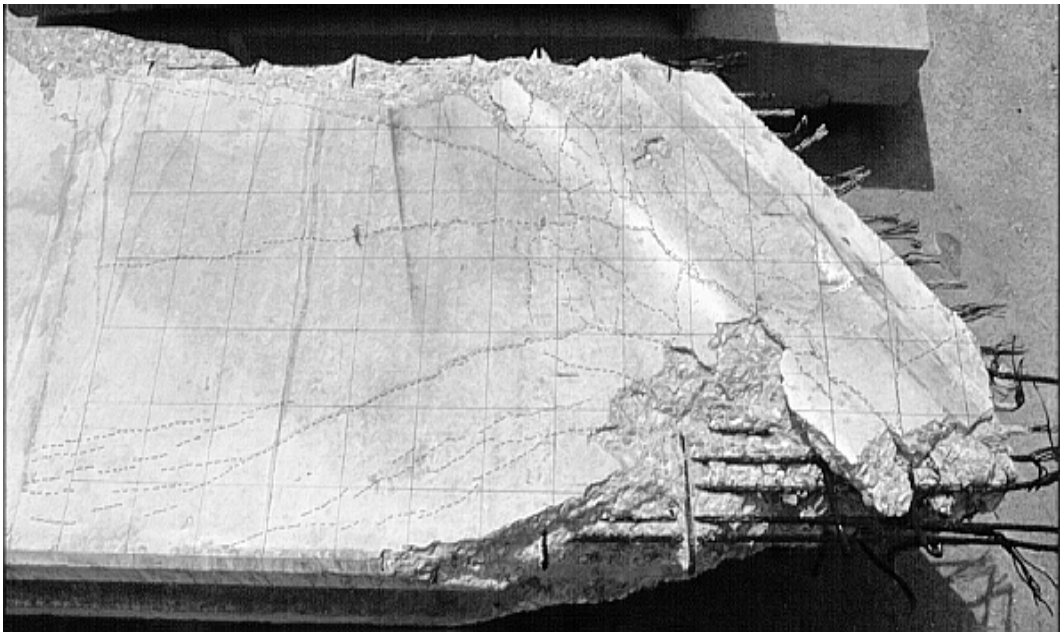

Figure D11: Photograph of Beam Underside, Box Beam 3 - Untested End

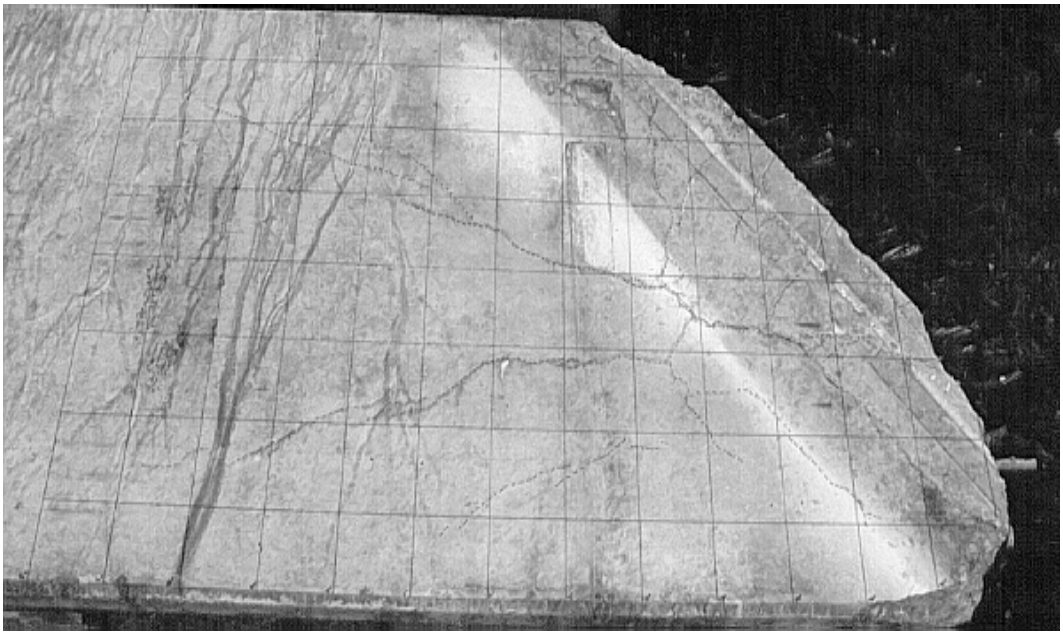

Figure D12: Photograph of Beam Underside, Box Beam 5 - Untested End

References

1. *AASHTO LRFD Bridge Design Specifications*, American Association of State Highway and Transportation Officials, Washington, D.C., 1994.

2. Bergmeister, K., Breen, J.E., Jirsa, J.O., and Kreger, M.E. "Design for Structural Detailing," Research Report 1127-3F, Center for Transportation Research, The University of Texas at Austin, May 1993.

3. Jaeger, B., Sansalone, M., and Poston, R. “Detecting voids in the grouted tendon ducts of post-tensioned structures,” ACI Structural Journal 93(4):462-73, 1996.

4. Lin, T.Y. and Burns, N.H., *Design of Prestressed Concrete Structures*, John Wiley and Sons, 1981.

5. *Plans of Proposed State Highway Improvement, U.S. Highway 287 - Tarrant County*, Sheets 164-174, State of Texas State Highway Department, 1974.

6. *Prestressed Concrete Box Beam Details BB28-1210 (4B28)*, MS18 Loading, Texas Department of Transportation Design Division (Bridge), 1997.

7. *Standard Specifications for Highway Bridges*, American Association of State Highway and Transportation Officials, Washington, D.C., 1996.